

DEVELOPMENT OF A COMPACT LIGHT DETECTION  
AND RANGING MODULE

NG KOK LEONG

MASTER OF ENGINEERING SCIENCE

FACULTY OF ENGINEERING AND GREEN  
TECHNOLOGY  
UNIVERSITI TUNKU ABDUL RAHMAN  
SEPTEMBER 2023

**DEVELOPMENT OF A COMPACT LIGHT DETECTION AND  
RANGING MODULE**

By

**NG KOK LEONG**

A dissertation submitted to the Department of Electronic Engineering,  
Faculty of Engineering and Green Technology,  
Universiti Tunku Abdul Rahman,  
in partial fulfillment of the requirements for the degree of  
Master of Engineering Science  
September 2023

## **ABSTRACT**

### **DEVELOPMENT OF A COMPACT LIGHT DETECTION AND RANGING MODULE**

**NG KOK LEONG**

Recent advancements in laser and detector technology have made it possible to create a compact Light Detection and Ranging, LiDAR system that is highly accurate and operates on low power. LiDAR systems consist of a laser source, photodetector, signal processor, and data processor. This research explores the potential of replacing the LiDAR Lite commercial unit's laser source with a smaller semiconductor laser. To achieve this, a complete prototype was developed using a miniature semiconductor laser called Vertical Cavity Surface Emitting Laser, VCSEL. The system was integrated with an Arduino UNO microcontroller and 3D-printed brackets. The laser used in the prototype is specifically characterized to meet the LiDAR system's requirements for laser power, wavelength, and beam shape. Testing was conducted in several stages to ensure the prototype's functionality. The data collected by the LiDAR prototype was analysed and presented as a Point Cloud, showing the position of points in X, Y, and Z coordinates. The system aims to provide a basis for future work.

## **ACKNOWLEDGEMENT**

I would like to thank everyone who had contributed to the successful completion of this project. I would like to express my gratitude to my research supervisor, Dr. Teh Peh Chiong and co-supervisor, Dr Yeap Kim Ho for their invaluable advice, guidance and their enormous patience throughout the development of the research.

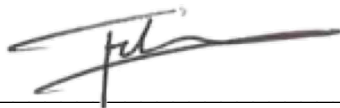
In addition, I would also like to express my gratitude to my loving parent and friends who had helped and given me encouragement.

This work was supported in part by UTAR research fund (project: IPSR/RMC/UTARRF/2016-C2/T05).

## APPROVAL SHEET

This dissertation entitled “**DEVELOPMENT OF A COMPACT LIGHT DETECTION AND RANGING MODULE**” was prepared by NG KOK LEONG and submitted as partial fulfilment of the requirements for the degree of Master of Engineering Science at Universiti Tunku Abdul Rahman.

Approved by:



\_\_\_\_\_  
(Dr. Teh Peh Chiong)  
Supervisor  
Department of Electronic Engineering  
Faculty of Engineering and Green Technology  
Universiti Tunku Abdul Rahman

Date: 7 September 2023



\_\_\_\_\_  
(Dr. Yeap Kim Ho)  
Co-supervisor  
Department of Electronic Engineering  
Faculty of Engineering and Green Technology  
Universiti Tunku Abdul Rahman

Date: 8 September 2023

## SUBMISSION SHEET

**FACULTY OF ENGINEERING AND GREEN TECHNOLOGY**

**UNIVERSITI TUNKU ABDUL RAHMAN**

Date: 7 September 2023

### SUBMISSION OF DISSERTATION

It is hereby certified that **NG KOK LEONG** (ID No: **17AGM05425**) has completed this dissertation entitled “**DEVELOPMENT OF A COMPACT LIGHT DETECTION AND RANGING MODULE**” under the supervision of Dr. Teh Peh Chiong (supervisor) from the Department of Electronic Engineering, Faculty of Engineering and Green Technology, and Dr. Yeap Kim Ho (Co-Supervisor) from the Department of Electronic Engineering, Faculty of Engineering and Green Technology.

I understand that University will upload softcopy of my dissertation in pdf format into UTAR Institutional Repository, which may be made accessible to UTAR community and public.

Yours truly,



---

(NG KOK LEONG)

## DECLARATION

I, NG KOK LEONG hereby declare that the dissertation is based on my original work except for quotations and citations which have been duly acknowledged. I also declare that it has not been previously or concurrently submitted for any other degree at UTAR or other institutions.



---

(NG KOK LEONG)

Date: 7 September 2023

## TABLE OF CONTENTS

	<b>Page</b>
<b>ABSTRACT</b>	iii
<b>ACKNOWLEDGEMENT</b>	iv
<b>APPROVAL SHEET</b>	v
<b>SUBMISSION SHEET</b>	vi
<b>DECLARATION</b>	vii
<b>TABLE OF CONTENTS</b>	viii
<b>LIST OF TABLES</b>	x
<b>LIST OF FIGURES</b>	xi
<b>LIST OF ABBREVIATIONS</b>	xiv
<b>LIST OF SYMBOLS</b>	xvi
<b>LIST OF PUBLICATIONS</b>	xviii
<b>CHAPTER 1</b>	<b>1</b>
<b>INTRODUCTION</b>	<b>1</b>
1.1 Objective	5
1.2 Thesis Arrangement and Outline	6
<b>CHAPTER 2</b>	<b>7</b>
<b>LITERATURE REVIEW</b>	<b>7</b>
2.1 Semiconductor Based Laser Diode	8
2.1.1 Vertical-Cavity Surface-Emitting Lasers	13
2.1.2 Edge Emitting Lasers (EELs)	15
2.1.3 Comparison of VCSEL and EELs	16
2.2 Semiconductor Photodetector	18
2.3 LiDAR Concept and Detection Technique	20
2.3.1 Time of Flight	20
2.3.2 Coherent and Incoherent LiDAR	22
2.4 Types of LiDAR	24
2.4.1 Mechanical Scanning LiDAR	24
2.4.2 Solid-State LiDAR	26
2.4.3 Fiber-based LiDAR	29
2.5 LiDAR Data Analysis & Visualise Tools	32
2.5.1 Point Cloud Library (PCL)	32
2.5.2 ArcGIS	33
2.6 LiDAR Data Format	34
2.6.1 LAS (LiDAR Data Exchange Format)	35
2.6.2 PCD (Point Cloud Data) Format	37
2.6.3 Comparison between PCD and LAS Format	39



<b>CHAPTER 3</b>	41
<b>LiDAR HARDWARE SETUP AND CHARACTERISATIONS</b>	41
3.1 Introduction to VCSEL	41
3.2 VCSEL for LiDAR application	45
3.3 VCSEL Laser Characterization	47
3.4 Implementation of VCSEL in LiDAR Setup	51
3.4.1 Measurement of Distance	54
3.4.2 Data Collection for a Single Plane	56
3.4.3 Setup for a 3-dimension Scanning (3D) LiDAR	58
<b>CHAPTER 4</b>	61
<b>LiDAR SOFTWARE AND IMAGING</b>	<b>61</b>
4.1 Collection of Point Cloud Data	64
4.1.1 Data Conversion from Polar to Cartesian Form	68
4.1.2 Arrangement of Data	69
4.1.3 Averaging of Data	70
4.1.4 Measurement Speed	73
4.1.5 Accuracy of the LiDAR Scanner	74
4.2 Point Cloud Data Conversion	80
4.2.1 Conversion tool program flow	81
4.2.2 User Interface Operating Flow	82
4.2.3 PCD Conversion Results	83
4.3 Visualisation of Point Clouds	85
<b>CHAPTER 5</b>	89
<b>CONCLUSION AND RECOMMENDATION</b>	<b>89</b>
5.1 Conclusion	89
5.2 Recommendation	91
<b>REFERENCES</b>	92
<b>APPENDICES</b>	99

## LIST OF TABLES

<b>Table</b>	<b>Page</b>
Table 2.1 Differences between VCSEL and EELs	17
Table 2.2: LAS Public Header Block (ASPRS, 2019)	36
Table 2.3: LAS Point Data Record Format 0 (ASPRS, 2019)	37
Table 2.4: Description of PCD data header.	38
Table 2.5: PCD vs LAS file format	40
Table 3.1 BOM list for LiDAR Setup	52
Table 4.1: The time taken for completing a single plane scanning with and without performing averaging.	73
Table 4.2: Comparison of controlled structure dimension of actual structure and point cloud measurement	78
Table 4.3: Header description for the converted .pcd file	84

## LIST OF FIGURES

<b>Figure</b>	<b>Page</b>
Figure 1.1: The configuration of LiDAR based on VCSEL	5
Figure 2.1: Typical architecture of LiDAR system consisting of semiconductor-based laser source and detector, optics configurations and data processing system	8
Figure 2.2: Physical mechanism of gain in a semiconductor laser involving absorption, spontaneous emission and stimulated emission.	10
Figure 2.3: Schematic of VCSEL (Iga, 2021)	14
Figure 2.4: Schematic of EELs (Iga, 2021)	15
Figure 2.5: Diagram of PIN diode with electric field distribution.	19
Figure 2.6: Diagram of APD with electric field distribution.	19
Figure 2.7: Time of flight concept applied to range measurement.	20
Figure 2.8: HDL-64E (Lidar, 2016)	25
Figure 2.9: Dimensions for medium Leddar Vu8 solid-state LiDAR configuration (LeddarTech, 2023)	27
Figure 2.10: Fully assembled solid-state LiDAR system by integrate Leddar Vu8 solid-state LiDAR sensor (Hagstedt and Jönsson, 2022)	28
Figure 2.11: the configuration of LiDAR based on fiber laser	30
Figure 2.12: PCD Header in Fixed Order	38
Figure 3.1: Schematic layer structure and operating principle of a VCSEL (Michalzik, 2013b)	41
Figure 3.2: Schematic diagram of 910nm VCSEL cross-sectional structure (Zhang et al., 2018)	42
Figure 3.3: Cross-sectional view of an oxidized GaAs VCSEL (Weigl et al., 1997)	43
Figure 3.4: Setup of a LiDAR Sensor with scanning rotation of 180 degree	46

Figure 3.5: VCSEL Laser Measurement Setup	47
Figure 3.6: Power-Current Characteristic of VCSEL PLA5506-940	48
Figure 3.7: Voltage-Current Characteristic of VCSEL PLA5506-940	49
Figure 3.8: Electrical Pulse and Optical Pulse Generated from VCSEL, pulse width 10us, repetition rate 100kHz.	50
Figure 3.9: The configuration of LiDAR based on VCSEL	51
Figure 3.10: Arduino Uno Microcontroller (Arduino, 2023)	53
Figure 3.11: Setup of VCSEL integrate into receiver module of the LiDAR Lite for distance measurement.	54
Figure 3.12: Graph of collecting 100 measurements by fixed the distance of LiDAR at 30cm from surface of an object	55
Figure 3.13: Graph of collecting 100 measurements by fixed the distance of LiDAR at 60cm from surface of an object	55
Figure 3.14: Setup of LiDAR unit mount on servo motor.	56
Figure 3.15: Scanning of LiDAR rotate 180-degree with servo motor	57
Figure 3.16: Plot of scanning LiDAR turning 180-degree in the platform build by pallet woods.	57
Figure 3.17: Setup of a 3D LiDAR with 3D printed holder.	58
Figure 3.18: 3D model for the LiDAR setup	59
Figure 3.19: Connections of the components	60
Figure 4.1: Point cloud of an environment (Ng, Lim and Teh, 2020)	61
Figure 4.2: Illustration of the interface between the components	64
Figure 4.3: Flow Chart of Arduino sketch to perform 3D scanning	66
Figure 4.4: Conversion of polar form to cartesian form	69
Figure 4.5: 10 Sample of LiDAR raw data recorded	69
Figure 4.6: Testing of 3D LiDAR scanning	70
Figure 4.7: Top view of point cloud scanning a single plane without performing averaging	71

Figure 4.8: Top view of point cloud scanning a single plane with performing averaging of 10 measurements	71
Figure 4.9: Top view of 3D Point Cloud scanning without performing averaging	72
Figure 4.10: Top view of 3D point cloud scanning with performing averaging of 10 measurements	72
Figure 4.11: Setup and actual dimensions for measurement of point cloud	74
Figure 4.12: Point Cloud of the controlled measurement structure	76
Figure 4.13: Measurement of the controlled structure	77
Figure 4.14: Flow chart of conversion .txt file to .pcd file	81
Figure 4.15: User interface of PCD conversion tool	82
Figure 4.16: User interface design flow for PCD conversion tool	83
Figure 4.17: Conversion from .txt file (left) to .pcd file (right)	84
Figure 4.18: 2D viewing of point cloud overlay on image	85
Figure 4.19: 3D viewing of point cloud	86

## LIST OF ABBREVIATIONS

2D	2-dimensions
3D	3-dimensions
APD	Avalanche photodiode
API	Application Programming Interface
AR	Augmented Reality
ArcGIS	Geographic Information System (GIS) software
ASCII	American Standard Code for Information Interchange
BOM	Build of Material
CAGR	Compound Annual Growth Rate
CW	Continuous wave
DBR	distributed Bragg reflector
DC	Direct Current
DTOF	Direct time of flight
EDFAs	Erbium Doped Fiber Amplifiers
EELs	Edge Emitting Lasers
FOV	Field of View
GIS	Geographic Information System
GND	Ground
GPS	Global Positioning System
I/O	Input or Output
IDE	Integrated Development Environment
IMU	Inertial Measurement Unit
iTOF	Indirect time of flight
LED	Light-Emitting Diode
LiDAR	Light Detection and Ranging
MEMS	Microelectromechanical systems
MQW	multiple-quantum-well
NIR	Near-infrared
PC	Personal Computer

PCD	Point Cloud Data
PCL	Point Cloud Library
PIN	Positive Intrinsic Negative
PWM	Pulse Width Modulation
QVGA	Quarter Video Graphics Array
QWs	Quantum Wells
RF	Radio Frequency
RGB	Red, Green and Blue
SPADs	single-photon avalanche diodes
SSL	Solid-state Laser
TOF	Time of Flight
UAV	Unmanned Aerial Vehicle
US	United State
USB	Universal Serial Bus
VCSEL	Vertical Cavity Surface Emitting Laser
VR	Virtual Reality

## LIST OF SYMBOLS

Al	Aluminium
AlGaAs	Aluminium Gallium Arsenide
As	Arsenic
$E_1$	Energy Level 1
$E_2$	Energy Level 2
Ga	Gallium
GaAs	Gallium Arsenide
In	Indium
N	Nitrogen
P	Phosphorus
Sb	Antimony
$c$	speed of Light
$L$	Length of the active medium
$n_g$	Refractive index of the active medium
$\Delta\nu_L$	Frequency mode spacing
A	Ampere
mA	milliampere
V	Volt
W	Watt
mW	milliwatt
cm	centimeter
$\mu\text{m}$	micrometer
nm	nanometer
$\mu\text{F}$	microfarad
$\text{k}\Omega$	kiloohm
s	second
$\mu\text{s}$	microsecond
kHz	kilohertz
m/s	meter per second



$\mu s/cm$	microsecond per centimeter
$d$	distance
$r$	distance
$\theta$	angle
$x_1$	x-coordinate of first point
$x_2$	x-coordinate of second point
$y_1$	y-coordinate of first point
$y_2$	y-coordinate of second point
$\backslash t$	tab
$\backslash s$	whitespace
$\backslash r$	Carriage returns

## LIST OF PUBLICATIONS

- (a) Teh, P.C., Lai, K.C., Hong, A.T.W., Leong, N.K. and En, O.C., 2017. LiDAR Point Cloud 3D attribute extraction and development of PCL based visualization interface. *i-manager's Journal on Cloud Computing*, 4(2), p.15.
  
- (b) Ng, K.L., Lim, W.X. and Teh, P.C., 2020. Implementation of 3D Mapping using A 2D LiDAR Scanner. *i-Manager's Journal on Electronics Engineering*, 10(3), p.1.

## CHAPTER 1

### INTRODUCTION

Light Detection and Ranging, or commonly known as LiDAR, is a remote sensing technology that uses light in the form of a pulsed to estimate and measure distance by illuminating a target and analysing the reflected light (Takeuchi et al., 1986; Campbell et al., 2002). The time it takes for the light pulse to travel to the target and back to the LiDAR system is measured by a photodetector. This time is directly proportional to the distance between the system and the object. This principle is commonly referred to as Time of Flight (TOF), and it allows for the calculation of distance based on the time taken for the pulse to travel back and forth.

The history of LiDAR technology can be traced back to the invention of laser in the early 1960s. It was first contributed to the application of meteorology, such as the measurement of gases, clouds, and aerosols (Wandinger, 2005). In 1971, the usage of laser altimeter to probe moon surface during the Apollo 15 mission triggered the attention of public about the accuracy and usefulness of the LiDAR system (Goyer and Watson, 1963; Liu et al., 2018). The high acquisition rate in spatial and temporal resolutions, powerful distance measurement capability, and the possibility of observing ambient atmospheric conditions have made the LiDAR instruments become the mainstream technology in airborne, meteorological, and terrestrial applications

for the past decades (Wandinger, 2005). For example, the prediction of range between aircraft to the target object, terrestrial vegetation, agriculture mapping, measurement of ozone fluxes, and so on (Nelson, 2013). Besides, due to the usage of 'laser', the amplitude backscatter reflectance energy in LiDAR instruments can be translated into useful information. This allows a greater opportunity for LiDAR in various research such as remote sensing on physical objects, feature classification and security surveillance system.

The advent of Industrial Revolution 4.0 has ushered in a new technological revolution in electronic-based sensors, with LiDAR leading the way. LiDAR technology is increasingly popular and widely applied to the next generation products such as in autonomous driving and also security industries. According to an analysis by Tommy, the autonomous car market in 2021 was valued at 22.22 billion US dollars and the market is predicted to reach 75.95 billion US dollars with a Compound Annual Growth Rate, CAGR of 22.75% in 2027 (Tommy Mi, 2022). LiDAR technology plays a critical role in enabling self-driving capabilities in autonomous vehicles. By detecting surroundings time in a fraction of a second and combining and used of powerful algorithm in software, the environment surrounding the vehicle can be mapped digitally (Levinson et al., 2011). Hence, enabling the vehicle to be driven automatically and avoid obstacles by using the digital map obtained via the LiDAR technique. This is why the LiDAR market, valued at 1.32 billion US dollars in 2018, is expected to increase to 6.71 billion US dollars, with a CAGR of 22.7% by 2026, according to Tommy's analysis.

A LiDAR instrument principally consists of a laser, a scanner, and specialized GPS receiver systems (Dethe, Shevatkar and Bijwe, 2011). The laser system usually occupied the largest space in the instrument since it is composed of laser and optical components (Bagley et al., 1998). Literature surveys reveal that most of the laser systems used are solid-state based (Lin and Liu, 2004). It required a dedicated chiller for the cooling purpose (Bagley et al., 1998). These characteristics and conditions in the laser system subsequently caused the commercial LiDAR instruments to be bulky in size, inefficient, and expensive to operate (Aho et al., 2017; Fersch, Weigel and Koelpin, 2017; Jeong, Hwang and Matson, 2018). Consequently, the main aim of this research study is to develop a LiDAR system that is compact in size and has laser capabilities equivalent to the solid-state based LiDAR. This eliminates the need for an external chiller, as air-cooling will be sufficient for the laser system. Besides, the compact system can be applied not only to road transport vehicles but also to the small drone/unmanned aerial vehicle (UAV). Moreover, the operation cost can be further reduced since the power requirement for a compact system is much lower than the bulky laser system. A LiDAR with high output power can measure and map surface with greater clarity and reduce the needs for very sensitive detection method (Ostermeyer et al., 2005). Currently, the available commercial compact LiDAR system from Velodyne is only capable of low power operation.

Research question: Bulky LiDAR, can it be scaled down?

This question is addressed through this research topic, evaluating the use of a new type of compact laser as the light source for the LiDAR.

Recently, semiconductor-based lasers, also known as semiconductor diode lasers, have played a significant role in the rapid development of laser technology. They are commonly used as pump sources for Erbium Doped Fiber Amplifiers (EDFAs) and find applications in a wide range of devices such as laser printers, barcode scanners, compact disc players, and telecommunication systems (Feng, Yang and Sun, 2021). Additionally, semiconductor lasers also have considerable usages in compact fiberized high-power laser systems. Due to their compactness and maintenance-free characteristics, these fiber lasers are dominated as the ideal candidate to replace those conventional bulk lasers (Dr. Rüdiger Paschotta, 2022). Moreover, their small footprints and all-fiber solution properties make them a suitable choice for modern compact products.

This study has chosen the Vertical-cavity surface-emitting laser (VCSEL) as the light source for the compact LiDAR system. VCSEL is a type of semiconductor laser diode that emits a laser beam perpendicular to the top surface and is suitable for LiDAR and sensing applications. The configuration of the LiDAR setup using VCSEL is as follows:

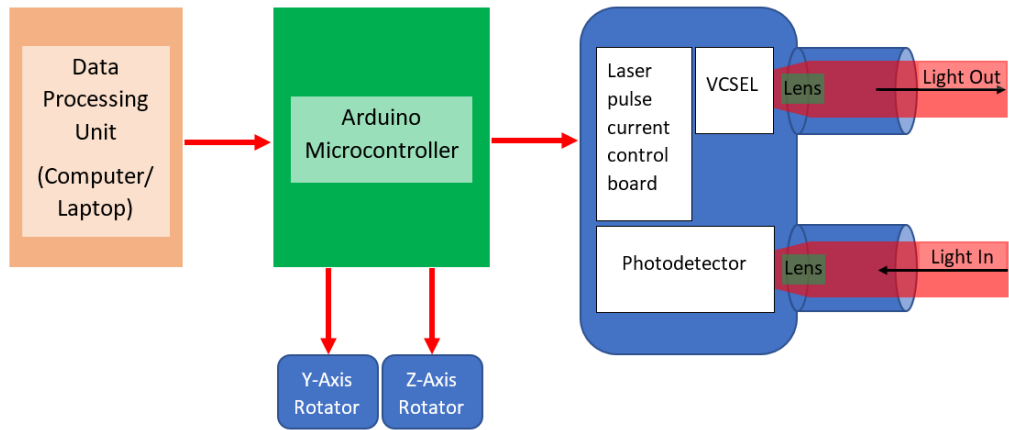


Figure 1.1: The configuration of LiDAR based on VCSEL

The measurement of a LiDAR system can be collected and organised in the form of point cloud. As Figure 1.1, a three-dimensional (3D) information can be obtained by getting the distance measurement information, sensor rotation angles and also the height data with the support of the Y and Z rotator. The operation and the data processing of the VCSEL based LiDAR system will be discussed in the following chapters.

## 1.1 Objective

The motivations behind this research work can be summarized as follows:

1. To develop a miniature laser module that can scan in 180 degrees in a single plane based on Light Detection and Ranging (LiDAR) concept.
2. To develop a data acquisition software for displaying the LiDAR measurement data.

## **1.2 Thesis Arrangement and Outline**

The thesis commences with Chapter One, which provides a brief introduction to the background of the research work and the motivation behind the use of VCSEL as a light source for a LiDAR module.

Chapter Two elucidates the fundamental theory and concept behind the LiDAR module, including its construction and implementation. Additionally, it reviews and discusses the current LiDAR data types and data characteristics in the literature.

Chapter Three presents a comprehensive discussion on the characteristics of a VCSEL and the design and construction of a VCSEL-based LiDAR module. It also covers the setup containing a microcontroller, along with the various testing and measurement results.

Chapter Four provides a detailed analysis and discussion of the data collected using the designed LiDAR module. The data is visualized in a user-friendly interface, with complete flexibility for data processing. This section also describes the method and data conversion process.

Finally, the last chapter summarizes the conclusions drawn from the research work and highlights future directions for further research.



## CHAPTER 2

### LITERATURE REVIEW

In recent years, LiDAR has become a popular piece of technology due to its precision, high resolution and excellent detection sensitivity. The advantages of using light instead of radio frequency (RF) is that light source utilizing short wavelength offers high resolution details and that such system is able to detect up to small particles in the air. With such high-resolution imaging offered by LiDAR, it has found useful applications in the field of engineering, meteorology, erosion and land slide monitoring, military usage and for autonomous vehicle applications. The deployment of LiDAR system is to be made possible as a result of the successful development of semiconductor technology. The basic LiDAR architecture consists a transmitter and a receiver and with the electronic driving circuits. The transmitter and receiver are normally semiconductor based, utilizing laser signal in the near-infrared wavelength.

This chapter will have a brief overview of the fundamental science involved in LiDAR operation. First, the fundamental properties of semiconductor laser diode are described and then followed up with the principle of photodiodes. Next, the fundamental principle for LiDAR based on TOF will be explained. The types of LiDAR system currently available in the market will be discussed next. Finally, the LiDAR data format and standard will be highlighted.

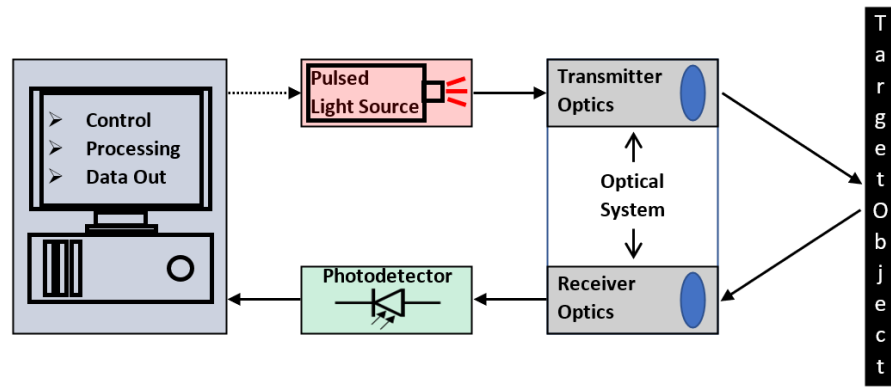


Figure 2.1: Typical architecture of LiDAR system consisting of semiconductor-based laser source and detector, optics configurations and data processing system

## 2.1 Semiconductor Based Laser Diode

One of the most important pieces of technology in laser technology is the semiconductor lasers. It consists of an active medium and the active medium is surrounded or sandwiched by n-type and p-type semiconductor materials (Kondow et al., 1997; Coleman, 2012). Generally, semiconductor lasers are derived from elements located in the third group (Al, Ga, In) and the fifth group (N, P, As, Sb) of the periodic table. N-type materials typically come from the fifth group, which have an available free electron, while p-type materials come from the third group, which have an empty hole. Since both the n-type and p-type materials are placed together, the free electron from the n-type material will fill the empty hole of the p-type material. Electron hole recombination results in lasing action, releasing energy in the form of optical radiation or photons at the junction of the materials. The wavelength of the emitted photons depends on the band-gap energy of the semiconductor materials used

(Yablonovitch and Kane, 1988). Lasing action involves three significant processes: photon absorption, spontaneous emission, and stimulated emission. Figure 2.2 illustrates these key processes in a simple two-energy-level diagram where  $E_1$  represents the ground-state energy and  $E_2$  represents the excited-state energy.

- i. Absorption in a semiconductor laser happens when a photon with enough energy pumps or excites a single electron from the valence band to the conduction band, where  $E_1$  and  $E_2$  represent the energy states of electrons in the valence and conduction bands, respectively. However, if the energy of the absorbed photon is lower than the energy difference between the two bands, electron excitation to the conduction band will not occur.
- ii. Spontaneous emission takes place when an electron in the conduction band recombines spontaneously with a hole in the valence band, emitting a photon with energy equivalent to the energy difference between the two bands.
- iii. Stimulated emission happens when an electron in the conduction band recombines with a hole in the valence band due to the presence of a photon with an equivalent band-gap energy. This process results in the generation of new photons, which are identical to the induced photons.

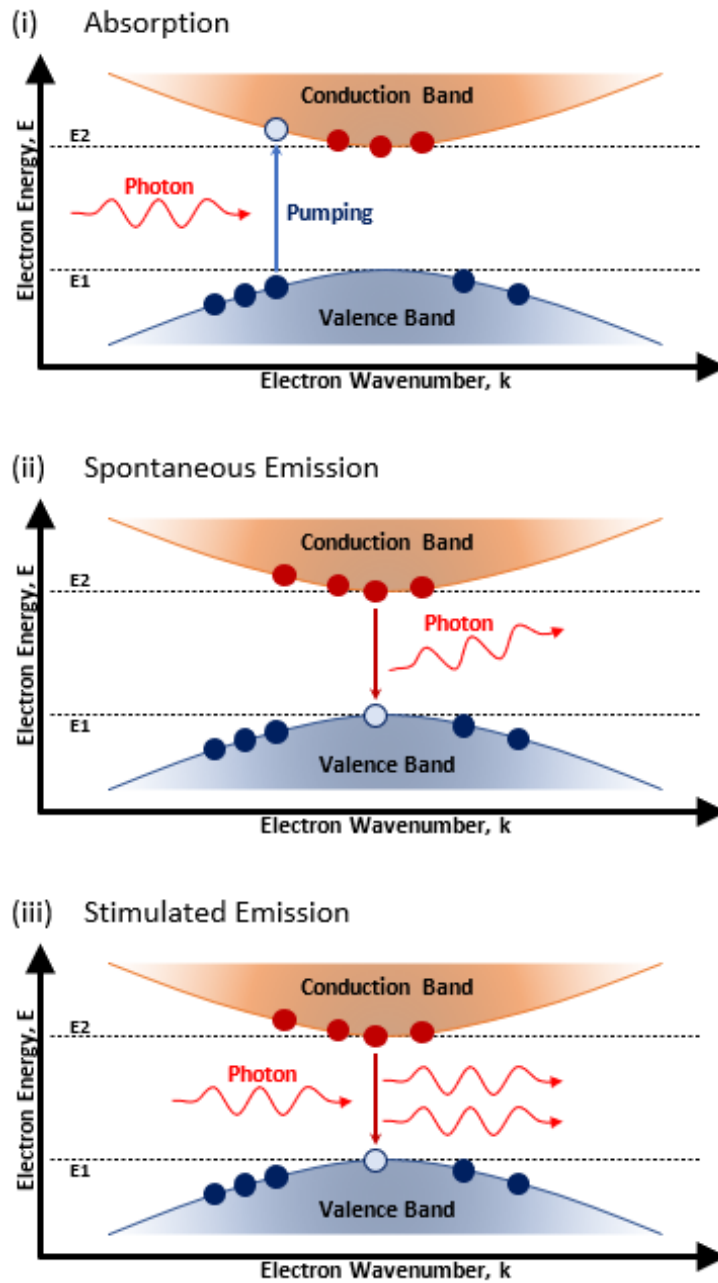


Figure 2.2: Physical mechanism of gain in a semiconductor laser involving absorption, spontaneous emission and stimulated emission.

When a semiconductor laser reaches a thermal equilibrium state, no lasing activity occurs because the number of electrons in the valence band is greater than the number of electrons available in the conduction band. In the event of an incident photon, the photon gets absorbed, eliminating the

possibility of stimulated emission. However, if the number of electrons available in the conduction band is higher than the number of electrons in the valence band, the stimulated emission process will dominate the absorption process, leading to lasing or optical gain. This situation, where the electrons in the conduction band outnumber those in the valence band, is called population inversion. Population inversion cannot occur unless external energy is fed to the valence band to excite the electrons to fill the conduction band. Such external energy comes from the external electrical pumping and is usually known as forward biasing p-n junction.

Relying solely on the pumping process for optical gain is not enough for lasing to occur. To achieve substantial lasing power at the output, a resonator with optical feedback is necessary. Typically, this is accomplished by placing polished end facets at both ends of the active medium, creating a Fabry-Perot cavity. The Fabry-Perot cavity has two functions: it determines the direction of the stimulated emission process and the longitudinal cavity modes (Yamada, 1983). This cavity produces standing waves for multiple frequencies, known as the longitudinal modes. The frequency mode spacing  $\Delta\nu_L$  is defined as followed:

$$\Delta\nu_L = \frac{c}{2n_g L}$$

$c$  : speed of light

$n_g$  : refractive index of the active medium

$L$  : length of the active medium

Using a longer cavity will result in the longitudinal modes being closely spaced together, increasing the number of modes within the emission band. However, this is not ideal for communication applications as it can cause dispersion in the transmitted signal along the fiber. Conversely, using a shorter cavity length increases the mode spacing while decreasing the number of longitudinal modes within the emission band.

In addition to longitudinal modes, spatial modes are also present in the semiconductor laser. These modes refer to the standing wave patterns that occur perpendicular to the direction of propagation in the cavity. The spatial modes have an impact on the far-field pattern of the laser emission. As the laser light exits from the output facet, it is diffracted due to the refractive index difference between the semiconductor material and the surrounding medium. This diffraction causes the laser beam to diverge in the far field, with different divergence angles in the vertical and horizontal directions. When a broad area laser is used, more spatial modes are excited, and higher-order transverse modes lead to increased beam divergence. As a result, the far-field pattern appears elliptical in shape. However, with a ridge waveguide, a smaller divergence angle is observed, thus resulting in far field pattern to be circular. Laser coupling into fiber will be more efficient and less loss with a circular pattern compared to elliptical pattern.

One major limitation of the semiconductor laser is the effect of temperature on the device's performance. It is known that excessive heating to the semiconductor laser will lead to catastrophic and irreversible damage. The damage observed at high device temperature is due to an increase in the rate of defect creation and propagation, which is directly dependent on the device temperature (Bou Sanayeh et al., 2007). Even though semiconductor laser is operating slightly below the temperature where the damage threshold, the lifetime of the laser will be affected. Apart from the damage due to temperature, laser parameters such as efficiency, wavelength and power stability, spatial modes and gain of the diode are also influenced by the device temperature.

### **2.1.1 Vertical-Cavity Surface-Emitting Lasers**

A VCSEL is a semiconductor laser that emits a circular output beam perpendicular to the wafer's surface, making it easy to integrate with other optical components. It is made up of a semiconductor material sandwiched between two mirrors that reflect light vertically (Iga, 2000). When an electric current passes through the device, it emits light from the top surface. Figure 2.3 illustrate the structure of a VCSEL.

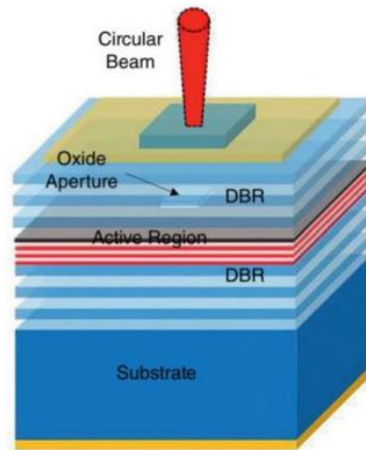


Figure 2.3: Schematic of VCSEL (Iga, 2021)

Since its invention in the 1980s, VCSELs have become widely used in data communications, sensing, industrial, and consumer electronics (Michalzik, 2013a). They have several advantages over other types of lasers, such as low power consumption, narrow beam divergence, and high modulation bandwidth (Zeng et al., 2017). They are also cost-effective to manufacture in high volume, making them ideal for mass production in data centres and consumer electronics (Zhou et al., 2017).

By introducing impurities, a p-n junction is formed in the semiconductor material situated between the mirrors. When an electric current passes through the p-n junction, it induces the recombination of electrons and holes, releasing energy in the form of photons. These photons reflect back and forth between the mirrors, gradually amplifying in intensity until they are emitted from the top surface as a coherent and focused light beam. (Iga, 2021).



VCSELs are highly efficient, consume low power, and have a narrow beam divergence, making them ideal for fiber-optic communication systems that transmit signals over long distances (Lavrencik, 2020). They are also compact and vertically emitted, allowing for easy integration with other optical components like lenses and detectors.

### 2.1.2 Edge Emitting Lasers (EELs)

EELs are a type of semiconductor laser diode that emit light from the edge of the semiconductor material. The structure of an EELs typically consists of a thin layer of semiconductor material sandwiched between two other layers of different semiconductor material, forming a p-n junction (Song, 2014). Figure 2.4 shows the structure of the EELs.

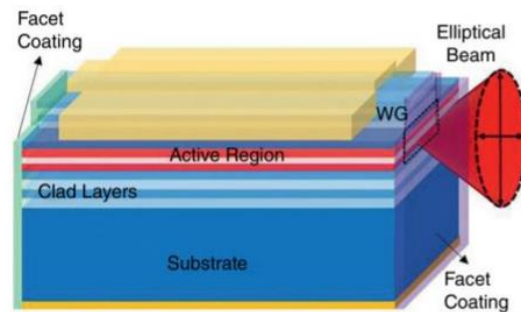


Figure 2.4: Schematic of EELs (Iga, 2021)

Passing an electric current through the p-n junction results in the recombination of electrons and holes, which in turn releases photons. These photons bounce back and forth between the reflective surfaces at the edges of the semiconductor material, gaining intensity with each reflection (FindLight, 2019). Finally, the photons that are emitted through one of the reflective

surfaces form a collimated beam of light that can be used for various applications. EELs are widely used in various applications such as fiber-optic communication systems, laser printing, barcode readers, and biomedical imaging.

EELs are typically more efficient than other types of lasers and can produce high-quality, collimated beams of light. However, they can be more difficult to manufacture than other types of lasers, and their output can be affected by temperature changes and other factors. Additionally, their output power is limited by the heat generated during operation, which can cause the laser to overheat and damage the semiconductor material (Paschotta, 2008b).

### **2.1.3 Comparison of VCSEL and EELs**

VCSELs and EELs (Edge Emitting Lasers) are both types of semiconductor lasers, but they have some differences in their design and performance that can impact their suitability for different applications. Here are some key differences between VCSELs and EELs:

Table 2.1 Differences between VCSEL and EELs

	VCSEL	EELs
Emitting Direction	emit light perpendicular to the surface of the semiconductor wafer	emit light parallel to the surface
Beam Quality	produce a more circular, symmetrical laser beam with less divergence	produce a narrow, elliptical beam of light
Wavelength Range	near-infrared (NIR) range	from the visible spectrum up to the mid-infrared range
Modulation Speed	high modulation speeds, typically ranging from several gigahertz up to several tens of gigahertz	Not as fast as VCSEL, typically be modulated at frequencies up to a few gigahertz
Power Consumption	Low power consumption, High efficiency	Higher power consumption than VCSEL
Cost	More expensive than EELs, due to high performance	Less Expensive, due to simpler manufacturing process

Overall, the choice between VCSELs and EELs will depend on the specific requirements of the application, such as range, precision, speed, power consumption, and cost. In general, VCSELs are a good choice for LiDAR applications that require high precision and fast response times, while EELs may be better suited for applications that require higher power or longer range.

## 2.2 Semiconductor Photodetector

The main function of a photodetector is to convert the incoming optical signal (both pulses and continuous wave) into an electrical signal. Photodetector is also known as Optical-Electrical Converter. As for semiconductor photodetector, they are commonly known as photodiodes and are widely used in optical communication systems due to its small form factor size, fast detection and high accuracy. Similar to the semiconductor-based laser diode, the construction of a semiconductor photodetector also relies on the p-type and n-type materials. However, unlike the semiconductor laser diode in which the PN junction is required to be forward-biased, the PN junction of a photodiode is reverse-biased. This is to ensure minimal current flowing in the diode during zero input signal.

Two common semiconductor photodetector which are widely used are known as Positive intrinsic Negative, PIN diode and Avalanche photodiode (APD). For a PIN diode, an intrinsic layer is normally placed in between the p-type and n-type materials and is responsible to enhance the quantum efficiency. As for an APD diode, the bias voltage is normally set to be very high so as to achieve maximum gain when photon amplification occurs. Figure 2.5 and 2.6 shows the electric field distribution of PIN diode and APD diode.

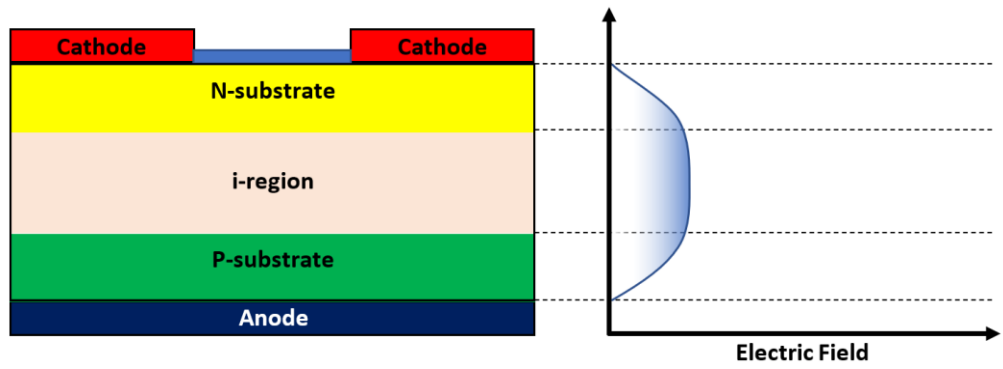


Figure 2.5: Diagram of PIN diode with electric field distribution.

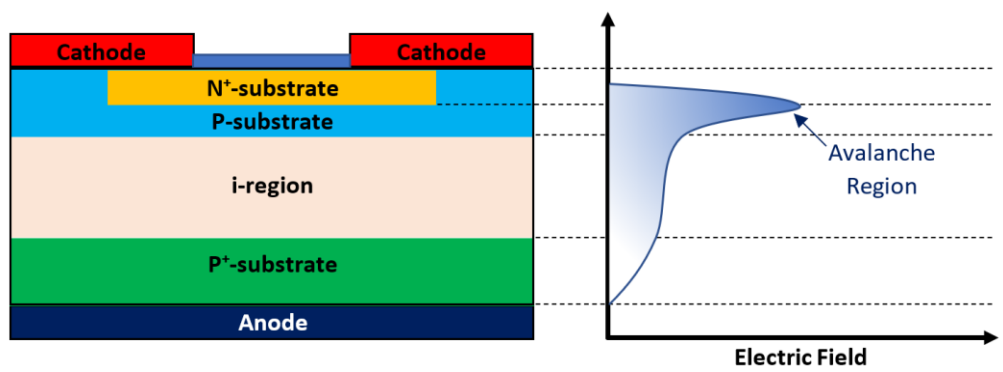


Figure 2.6: Diagram of APD with electric field distribution.

## 2.3 LiDAR Concept and Detection Technique

### 2.3.1 Time of Flight

Time of flight is a fundamental concept in LiDAR systems. It is primarily based on time measurement for a wave to propagate from the source point to an object and get reflected back to the origin. Based on the time measurement and the law of physics, the distance of the object from the source can be calculated and determined. Various types of travelling waves can be used, but the most effective and popular will be the light signal, either directly from a laser source or a LED source. Figure 2.7 illustrated the time of flight concept.

$$Distance = \frac{speed\ of\ light\ \times\ time}{2}$$

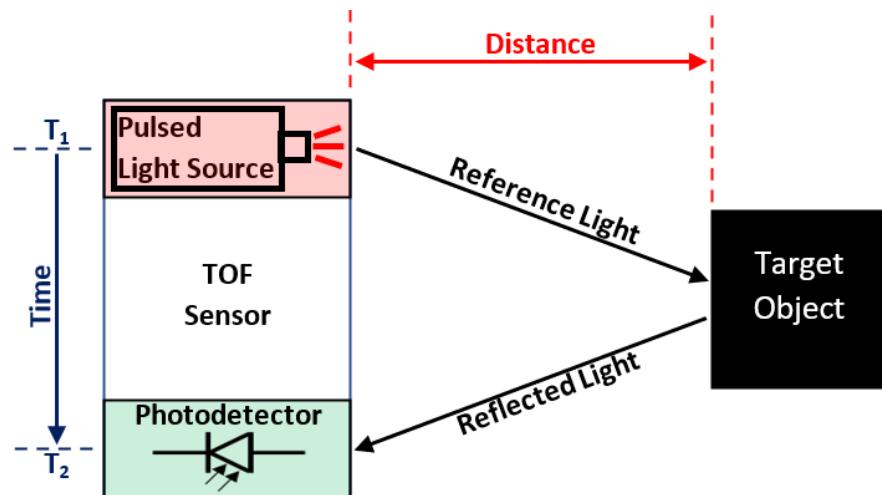


Figure 2.7: Time of flight concept applied to range measurement.

LiDAR systems based on TOF have become increasingly popular in recent years, particularly in the fields of autonomous vehicles, robotics, and environmental monitoring. TOF LiDAR systems offer several advantages over other LiDAR systems, including high accuracy, robustness to ambient lighting, and the ability to measure long distances.

TOF is a critical parameter in the design and performance of LiDAR systems. The accuracy of TOF measurements depends on several factors, including the timing resolution of the measurement device, the quality of the laser source, and the reflectivity of the target object. By optimizing these factors, LiDAR systems can achieve high accuracy and precision in distance measurements.

Besides, there has been significant research and development in the field of LiDAR, with a focus on improving the performance and reducing the cost of TOF-based systems. According to a review article by Mester et al., 2018, advances in laser technology, signal processing, and machine learning have led to significant improvements in the accuracy, speed, and cost-effectiveness of LiDAR systems based on TOF.

Overall, the concept of TOF is a fundamental principle in LiDAR systems and plays a critical role in functioning and optimization of these systems. Advances in laser technology, signal processing, and machine learning are likely to lead to further improvements in the accuracy and cost-effectiveness of

TOF-based LiDAR systems, making them an increasingly important tool in many fields.

### **2.3.2 Coherent and Incoherent LiDAR**

Coherent and incoherent LiDAR are two different techniques used in LiDAR remote sensing technology that uses laser pulses to measure distances and generate 3D representations of objects and environments. Both coherent and incoherent LiDAR have their unique characteristics and applications.

Coherent LiDAR systems use lasers that produce a continuous wave (CW) or a pulse with a narrow linewidth and a well-defined phase. The laser beam is then modulated in some way, such as by frequency shifting, to encode information about the distance and velocity of the targets in the environment (Menzies, 1985; Photonics Report, 2022). Coherent LiDAR can achieve high spatial resolution and range accuracy, but can be more complex and expensive than incoherent LiDAR.

Incoherent LiDAR systems use lasers that produce a pulse with a broader linewidth and less well-defined phase than a coherent laser. The reflected light from the pulse is detected and the time delay between the emitted pulse and the detected signal is used to determine the distance to the target (Menzies, 1985; Photonics Report, 2022). Incoherent LiDAR systems are typically simpler and less expensive than coherent LiDAR, but may have lower



range resolution and accuracy.

In general, coherent LiDAR is well-suited for applications that require high accuracy and precision, such as atmospheric remote sensing or long-range detection and tracking of objects. Incoherent LiDAR, on the other hand, is well-suited for applications that require simplicity, low cost, and relatively short range, such as automotive safety systems or robot navigation.

## **2.4 Types of LiDAR**

### **2.4.1 Mechanical Scanning LiDAR**

Mechanical LiDAR, also known as scanning LiDAR, is one of the earliest and well-established types of LiDAR systems. It operates by using a rotating mirror or prism to scan a laser beam across the target area. The reflected light is then detected by a sensor, typically a photodetector, and this data is utilized to construct a detailed 3D image of the scanned environment. Mechanical LiDAR systems are known for their precision and longer detection ranges (Royo and Ballesta-Garcia, 2019).

In a mechanical LiDAR system, the rotating mirror or prism plays a crucial role in deflecting the laser beam across the target area. By measuring the angle of deflection and the time delay between the emission of the laser pulse and the detection of the reflected light, the distance to the objects in the area can be accurately calculated. This scanning process enables the generation of a comprehensive 3D map of the entire target region.

One of the primary advantages of mechanical LiDAR systems is their high resolution and accuracy. They excel in capturing detailed information, making them suitable for various applications such as surveying, mapping, and remote sensing. Additionally, mechanical LiDAR can perform effectively in adverse environmental conditions, including rain, fog, and snow.

However, mechanical LiDAR systems have certain drawbacks. They tend to be larger, more complex, and relatively expensive compared to solid-state LiDAR systems (Chung, Abediasl and Hashemi, 2017). Their mechanical components also make them more prone to wear and mechanical failures, requiring regular maintenance. As solid-state LiDAR technology has rapidly advanced, mechanical LiDAR is gradually being replaced by more compact, reliable, and cost-effective solid-state LiDAR systems.

The example of the current commercially available mechanical LiDAR system is Velodyne HDL-64E, as shown in figure 2.8. It is a mechanical LiDAR system with a rotating assembly that spans approximately 406mm (16 inches) in diameter and 254mm (10 inches) in height. Based on the data specification, HDL-64E offers high accuracy, capable of capturing precise 3D point cloud data with distance accuracy within 2cm, making it suitable for applications such as object detection and navigation. The system's 64 laser beams provide a 360-degree field of view, generating a dense point cloud that can be visualized using specialized software for detailed environmental mapping and analysis, aiding in identifying objects and surfaces based on intensity or distance (Lidar, 2016).



Figure 2.8: HDL-64E (Lidar, 2016)

Despite the shift towards solid-state LiDAR, mechanical LiDAR still finds valuable applications in specific scenarios that demand high precision and accuracy. As the LiDAR technology continues to evolve, a diverse range of industries will benefit from the continued advancements in both mechanical and solid-state LiDAR systems, ensuring improved data collection and analysis capabilities for various fields and applications.

#### **2.4.2 Solid-State LiDAR**

Solid-state LiDAR is a cutting-edge LiDAR technology that overcomes several limitations associated with traditional mechanical scanning LiDAR systems. It achieves this by using solid-state components like solid-state diode lasers (SSL) and photodetectors to emit and receive laser pulses. The development of solid-state LiDAR is driven by the need to address challenges related to cost, size, reliability, and complexity often encountered in mechanical scanning LiDAR systems (López, Mahony and Kim, 2020).

In contrast to mechanical LiDAR systems that rely on moving parts to scan the environment, solid-state LiDAR systems utilize electronic scanning mechanisms, such as microelectromechanical systems (MEMS), to create a 3D map of the surrounding environment. While solid-state LiDAR offers numerous advantages, its field-of-view (FOV) coverage is typically limited to around 90 to 120 degrees, which may not meet the requirements of certain applications (Davis et al., 2016). To expand the coverage area and cater to specific

application needs, it may be necessary to combine two or more solid-state LiDAR sensors.

The Leddar Vu8 is a solid-state LiDAR module designed by LeddarTech, a leading player in LiDAR technology innovation. Compact and versatile, the Leddar Vu8 module offers capabilities for object detection and ranging in a variety of applications. Figure 2.9 shows a medium range Leddar Vu8 sensor with dimensions of approximately 49.6mm in width, 35.9mm in length and 70mm in height, the Leddar Vu8 is engineered to fit seamlessly into diverse environments. It can achieve the measurement with accuracy of  $\pm 5\text{cm}$  and precision of  $\pm 6\text{mm}$  (LeddarTech, 2023). In 2022, Christian Hagstedt and Sebastian Jönsson reported the design of a solid-state LiDAR system by using Leddar Vu8 as the LiDAR sensor for the system. The overall dimension for the LiDAR system is approximately 180mm in length, 90mm in width and height is 95mm. Figure 2.10 shows the designed solid-state LiDAR system.

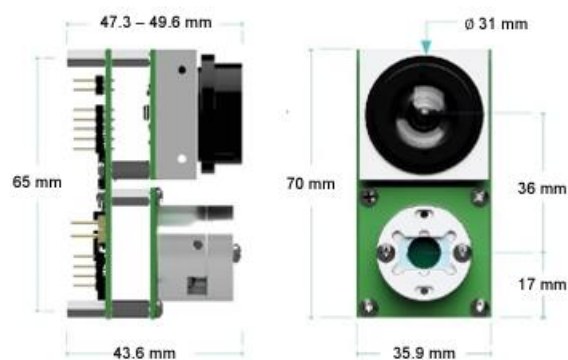


Figure 2.9: Dimensions for medium Leddar Vu8 solid-state LiDAR configuration (LeddarTech, 2023)

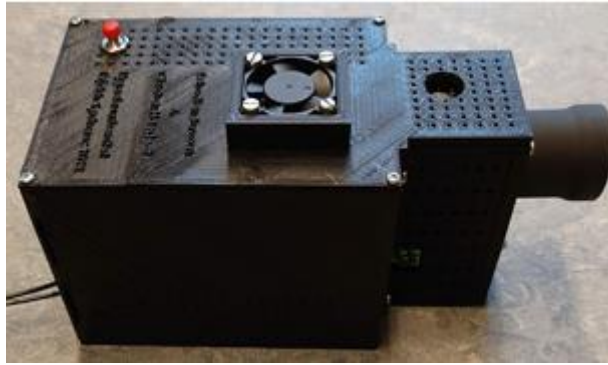


Figure 2.10: Fully assembled solid-state LiDAR system by integrate Leddar Vu8 solid-state LiDAR sensor (Hagstedt and Jönsson, 2022)

One particular advancement within solid-state LiDAR technology is high-power solid-state LiDAR. These systems employ a combination of high-power lasers, high-speed scanning mechanisms, and advanced optics to achieve long-range, high-resolution sensing capabilities. As a result, high-power solid-state LiDAR finds ideal applications in fields like autonomous vehicles and drones, where extended sensing range is crucial for safe and efficient operation.

However, it is essential to consider some trade-offs associated with high-power solid-state LiDAR systems. They tend to be more expensive and complex compared to standard solid-state LiDAR systems due to the advanced components required for high-power operation. Additionally, high-power systems demand more power, which can pose challenges in certain applications where power efficiency is critical. Some high-power solid-state LiDAR systems may even necessitate a chiller to cool the laser diodes, particularly when operating at high power levels. This cooling is crucial to maintain the temperature of the diodes within a specified operating range, ensuring reliable performance and preventing damage to the components (Bagley et al., 1998).

### **2.4.3 Fiber-based LiDAR**

The availability of compact, fiberized high-power laser systems is rapidly gaining popularity in the field of laser-based products. These fiber lasers offer a maintenance-free and compact alternative to bulky conventional lasers, making them an ideal candidate for replacing outdated laser technologies (Kameyama et al., 2007). With their small footprints and all-fiber solutions, they are particularly well-suited for modern compact products (Ong et al., 2013).

Fiber-based LiDAR has emerged as a superior technology compared to solid-state and mechanical LiDAR in various aspects. One of its notable advantages is the longer detection ranges it can achieve. This can be attributed to the use of optical fibers, which efficiently transmit and maintain laser signals over extended distances, allowing for enhanced range capabilities. Additionally, fiber-based LiDAR provides high spatial resolution, enabling the detection of smaller objects and enabling detailed environmental mapping.

The flexibility offered by optical fibers is another significant advantage of fiber-based LiDAR. It allows for easier integration into different designs and installation scenarios, providing greater adaptability to diverse applications. Moreover, these LiDAR systems boast a compact and lightweight design, making them easy to install on various platforms, including vehicles, drones, and other mobile devices.

The reliability of fiber-based LiDAR systems is further enhanced by their fewer moving parts. Unlike mechanical LiDAR systems, which involve rotating components that may be prone to wear and mechanical failures, fiber-based LiDAR's design minimizes such risks. As a result, these systems require less maintenance and offer a more dependable solution for continuous operation.

Figure 2.11 showcases a setup utilizing a fiber-based laser, which can be upgraded to support high-power operations through a pulsed-based fiber laser system.

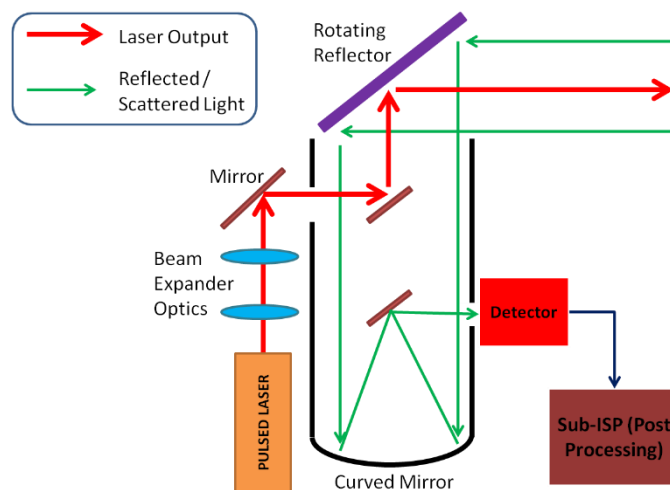


Figure 2.11: the configuration of LiDAR based on fiber laser

Such an upgraded module has extensive applications, including advanced surveying and environmental monitoring (e.g., haze, forest fires, pollution monitoring) (Lee, Wei and Guo, 2017). Furthermore, fiber-based LiDAR is finding increasing importance in the development of autonomous cars and self-driving vehicles, where precise and long-range sensing is crucial for safe navigation and obstacle detection.



Next, the various data formats for the LiDAR are discussed. The data collected from the LiDAR hardware will need to be converted to the appropriate formats to enable the data to be analysed. Analysis of the LiDAR data can use widely available third-party software such as ArcGIS, an open-source software which will be introduced in the next part (Singh and Bawa, 2016; Szewrański et al., 2017; Koo, Chun and Griffith, 2018).

## **2.5 LiDAR Data Analysis & Visualise Tools**

### **2.5.1 Point Cloud Library (PCL)**

Point Cloud Library (PCL) is an open-source software library written in C++ that provides a modular architecture and a rich set of algorithms for processing 3D point cloud data. Point clouds represent 3D surfaces of physical objects or environments and can be obtained from a variety of sources, such as 3D scanning or LiDAR (Rusu and Cousins, 2011).

PCL's algorithms enable developers to perform operations on point clouds such as filtering, feature extraction, registration, segmentation, and surface reconstruction (Rusu and Cousins, 2011). The library is compatible with many 3D sensors and supports a variety of file formats for reading and writing point cloud data.

PCL is used in various applications, including robotics, autonomous driving, augmented reality, and 3D modelling. For example, PCL can help a robot navigate its environment by identifying obstacles and planning safe paths, or it can be used to create 3D models of buildings for architectural or engineering purposes. Overall, PCL is a powerful and popular tool for working with 3D point cloud data.

### 2.5.2 ArcGIS

ArcGIS is a Geographic Information System (GIS) software platform that provides a suite of tools and applications for managing, analysing, and visualizing spatial data (Booth and Mitchell, 2001). Among its features are tools for point cloud processing that allow users to work with point cloud data from different sources and import it in various formats, including LAS, LAZ, and ASCII. Once imported, the data can be filtered and classified based on criteria like elevation, intensity, or colour, and users can extract specific features such as buildings or trees.

In addition, ArcGIS includes tools for visualizing point cloud data in 3D views and orthoimage, giving users the ability to explore and analyse data from multiple angles and perspectives. The software also provides an extensive range of tools for spatial analysis, data management, and visualization, including proximity analysis, network analysis, and spatial statistics (Li, Hodgson and Li, 2018). Users can visualize spatial data in various formats like interactive maps, 3D scenes, and dashboards.

Overall, ArcGIS is a comprehensive GIS software platform that allows professionals to integrate and analyse spatial data from diverse sources, perform complex spatial analysis, and visualize results in various formats. It is a valuable tool for professionals who rely on spatial data to make informed decisions. However, a license is required to use the software for point cloud processing.

## 2.6 LiDAR Data Format

As LiDAR technology advances, larger LiDAR datasets require proper data handling techniques. Selecting the appropriate data format for translating between various software and ensuring compatibility is essential for effectively managing these datasets. The most prevalent LiDAR data formats are LAS, LAZ, ASCII, XYZ, and E57, which are utilized to store point cloud data containing GPS coordinates, RGB colour values, and point classification. LAS and LAZ are binary formats that offer high compression for efficient storage and sharing, while ASCII and XYZ are text-based formats that can be easily edited, but may result in larger file sizes (Winiwarter et al., 2022). E57 is specifically designed for 3D imaging data, including LiDAR data, and provides high compression for easy sharing across different software platforms (Im, Baek and Lee, 2016). Another commonly used format for storing LiDAR data is PCD (Point Cloud Data), which is prevalent in the robotics and autonomous vehicle industries due to its ability to efficiently store large point clouds with various attributes such as RGB colour values, point normal, and curvature (Wu et al., 2021). It is essential to consider the specific requirements of each application and select the appropriate LiDAR data format accordingly.

### **2.6.1 LAS (LiDAR Data Exchange Format)**

LAS is a binary file format used to store LiDAR point cloud data obtained from airborne LiDAR systems. It is a specialized format designed to handle large amounts of point cloud data (ASPRS, 2019; Rock Academy, 2023).

A LAS dataset is a collection of LAS files that are associated with a specific LiDAR survey. It may consist of one or more LAS files covering a specific geographic region or area. The organization of the LAS dataset may vary depending on the project requirements, but it generally contains metadata such as project information, geographic location, data quality, and data processing parameters. The LAS dataset may also include different levels of point cloud data, such as raw point clouds, filtered point clouds, and point clouds classified into different categories based on terrain, vegetation, or man-made objects (ArcMap, 2023).

The LAS file format consists of two parts: the header and the point records. The header contains information about the LAS file, such as the format version, the number of points in the file, the scale factor for the X, Y, and Z coordinates, and other information about the LiDAR survey. The point records section of the LAS file contains the individual LiDAR measurements, each represented by a point record that includes the X, Y, and Z coordinates of the point, the intensity value, and the classification code. The LAS format also supports various data compression techniques to reduce the file size while preserving the accuracy of the data (Isenburg, 2013; ASPRS, 2019).

Table 2.2: LAS Public Header Block (ASPRS, 2019)

Item	Format	Size	Required
FileSignature("LASF")	char[4]	4bytes	yes
FileSourceID	unsignedshort	2bytes	yes
GlobalEncoding	unsignedshort	2bytes	yes
ProjectID-GUIDData1	unsignedlong	4bytes	
ProjectID-GUIDData2	unsignedshort	2bytes	
ProjectID-GUIDData3	unsignedshort	2bytes	
ProjectID-GUIDData4	unsignedchar[8]	8bytes	
VersionMajor	unsignedchar	1byte	yes
VersionMinor	unsignedchar	1byte	yes
SystemIdentifier	char[32]	32bytes	yes
GeneratingSoftware	char[32]	32bytes	yes
FileCreationDayofYear	unsignedshort	2bytes	yes
FileCreationYear	unsignedshort	2bytes	yes
HeaderSize	unsignedshort	2bytes	yes
OffsettoPointData	unsignedlong	4bytes	yes
NumberOfVariableLengthRecords	unsignedlong	4bytes	yes
PointDataRecordFormat	unsignedchar	1byte	yes
PointDataRecordLength	unsignedshort	2bytes	yes
LegacyNumberOfPointRecords	unsignedlong	4bytes	yes
LegacyNumberOfPointbyReturn	unsignedlong[5]	20bytes	yes
XScaleFactor	double	8bytes	yes
YScaleFactor	double	8bytes	yes
ZScaleFactor	double	8bytes	yes
XOffset	double	8bytes	yes
YOffset	double	8bytes	yes
ZOffset	double	8bytes	yes
MaxX	double	8bytes	yes
MaxY	double	8bytes	yes
MaxZ	double	8bytes	yes
MinX	double	8bytes	yes
MinY	double	8bytes	yes
MinZ	double	8bytes	yes
StartofWaveformDataPacketRecord	unsignedlonglong	8bytes	yes
StartofFirstExtendedVariable LengthRecord	unsignedlonglong	8bytes	yes
NumberOfExtendedVariable LengthRecords	unsignedlong	4bytes	yes
NumberOfPointRecords	unsignedlonglong	8bytes	yes
NumberOfPointsbyReturn	unsignedlonglong[15]	120bytes	yes

Table 2.3: LAS Point Data Record Format 0 (ASPRS, 2019)

Item	Format	Size	Required
X	long	4 bytes	yes
Y	long	4 bytes	yes
Z	long	4 bytes	yes
Intensity	unsigned short	2 bytes	no
Return Number	3 bits (bits 0-2)	6 bytes	yes
Number of Returns (Given Pulse)	3 bits (bits 3-5)	3 bits	yes
Scan Direction Flag	1 bit (bit6)	1 bit	yes
Edge of Flight Line	1 bit (bit 7)	1 bit	yes
Classification	unsigned char	1 byte	yes
Scan Angle Rank (-90 to +90) Left Side	signed char	1 byte	yes
User Data	unsigned char	1 byte	no
Point Source ID	unsigned short	2 bytes	yes
Minimum PDRF Size		20 bytes	

### 2.6.2 PCD (Point Cloud Data) Format

PCD format is a file format for storing 3D point cloud data in a structured manner. It was developed by the PCL project and has become a widely adopted standard for storing and processing point cloud data.

The PCD format supports both ASCII and binary encoding, and can store a variety of information for each point, such as position, colour, intensity, and normal vectors (Point Cloud Library, 2023). This makes it a very flexible and versatile file format for storing 3D data from a variety of sources, including LiDAR, structured light scanners, and RGB-D cameras (Kim and Cho, 2020).

The structure of a PCD file is defined by a header that contains metadata about the point cloud, such as the number of points, the point type, and the dimensions of the point cloud (Point Cloud Library, 2023). The header is followed by the actual data, which is stored as a series of point records. Each point record contains the data for a single point, including its coordinates and any associated attributes. Figure 2.12 shows the typical example of a PCD data header and Table 2.4 describe the components in the header.

```

1 VERSION
2 FIELDS → FIELDS x y z           # XYZ data
3 SIZE     FIELDS x y z rgb      # XYZ + colors
4 TYPE     FIELDS x y z normal_x normal_y normal_z # XYZ + surface normals
5 COUNT    FIELDS j1 j2 j3      # moment invariants
6 WIDTH
7 HEIGHT
8 VIEWPOINT
9 POINTS
10 DATA

```

Figure 2.12: PCD Header in Fixed Order

Table 2.4: Description of PCD data header.

Header Components	Description
VERSION	Specifies the version of the PCD file format being used.
FIELDS	Defines the attribute fields of each point in the point cloud.
SIZE	Indicates the size (in bytes) of each attribute.
TYPE	Specifies the data type of each attribute.
COUNT	Indicates the number of elements per attribute.
WIDTH	Denotes the number of points in each row of the point cloud.
HEIGHT	Represents the number of rows in the point cloud. For unorganized point clouds, this value is typically set to 1.
VIEWPOINT	Specifies the viewpoint of the camera used to capture the point cloud.
POINTS	Indicates the total number of points in the point cloud.
DATA	Specifies the format of the point data.



One of the benefits of the PCD format is that it is widely supported by software packages in the point cloud processing community, including the Point Cloud Library (PCL), CloudCompare, and MeshLab (mmolero, 2022). This makes it easy to exchange point cloud data between different software packages and to work with point cloud data across different applications.

In addition to its flexibility and ease of use, the PCD format also has a relatively small file size compared to other formats, making it well suited for storing and transferring large point clouds. Overall, the PCD format is a powerful tool for storing and processing point cloud data, and is a key component of many applications in fields such as robotics, computer vision, and 3D scanning (Chickerur and Joshi, 2015).

### **2.6.3 Comparison between PCD and LAS Format**

Table 2.5 highlights the major features that distinguish PCD and LAS formats. LAS is an industry standard designed to facilitate LiDAR data exchange between vendors and is often used in workflows for terrain and mosaic datasets. LAS files are typically bundled in sets that complement these workflows. On the other hand, PCD is focused on user-friendliness and provides easy accessibility to point cloud data through its support for ASCII data types that can be directly plotted. PCD also offers flexibility in terms of its usage within the Point Cloud Library (PCL) ecosystem.

Table 2.5: PCD vs LAS file format

<b>Specification</b>	<b>PCD</b>	<b>LAS</b>
Data Structure	Organized point cloud datasets in row and column structure, improves efficiency of nearest neighbour operation	Bundle of LAS files build from group of LiDAR data, eg: GPS, IMU etc
Data Type	ASCII or Binary (mmap/munmap)	Binary (Little Endian)
Features	n-D histograms for feature descriptors, full control of file format	Scalable dataset that enables quick statistical analysis
Display	Point cloud	Surface or point cloud
Types of LiDAR	Airborne and terrestrial	Airborne and terrestrial
Storage Location	File system	File system
Analysis	Use with PCL engine	Use with LAS dataset tools, eg: LAS file viewer, Qt Reader, ArcGIS, CloudCompare

## CHAPTER 3

### LIDAR HARDWARE SETUP AND CHARACTERISATIONS

#### 3.1 Introduction to VCSEL

The VCSEL is a type of semiconductor laser diode that emits light vertically from its top surface, rather than from the side edge like traditional edge-emitting lasers (EELs) (Kaplan, 2007). Compared to EELs, VCSELs offer several advantages such as lower threshold current, higher efficiency, and easy integration with other optical components (Koyama, 2006; Larsson and Gustavsson, 2013). The laser light in a VCSEL propagates or emits in the vertical direction of the surface of the semiconductor wafer, whereas in EELs, the light is emitted in the direction along the wafer surface of the semiconductor chip, and the laser beam is usually reflected or coupled out at a cleaved edge (Koch and Hofmann, 2018).

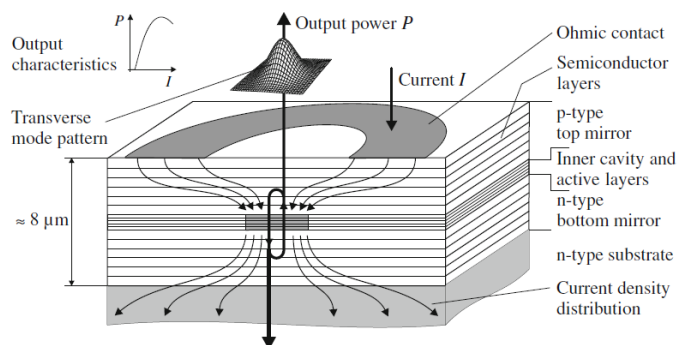


Figure 3.1: Schematic layer structure and operating principle of a VCSEL

(Michalzik, 2013b)

Figure 3.1 depicts the standard structure of a VCSEL, which consists of three main components: the active layers, n-type substrate, and p-type substrate (Bragg reflector). The active region, which is responsible for generating laser light, consists of one or a few quantum wells (QWs) sandwiched between the n-type and p-type Bragg reflector mirrors that are parallel to the wafer surface, forming a laser resonator (Zhang et al., 2018). The bottom n-type Bragg reflector has a low refractive index to achieve high reflectivity, while the top p-type reflector has a lower reflectivity, allowing some lasing light to escape from the device and reflecting some light back to the quantum well (Weigl et al., 1997; Seurin et al., 2009). This bouncing of photons between the top and bottom reflectors causes them to combine and emit the recombination energy as light, resulting in the formation of the laser in the quantum well. This is the typical lasing mechanism in all lasers (Michalzik, 2013b).

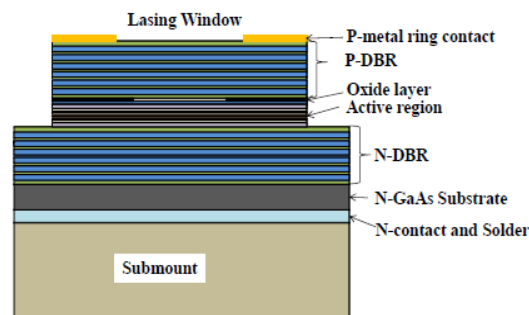


Figure 3.2: Schematic diagram of 910nm VCSEL cross-sectional structure (Zhang et al., 2018)

VCSELs can generate wavelengths ranging from 650 to 1300nm using the active region, or quantum well, typically made of gallium arsenide (GaAs) and aluminium gallium arsenide (AlGaAs). The quantum well comprises two

thick AlGaAs layers sandwiching a very thin GaAs layer, which restricts electron movement in the vertical Z direction and increases lasing efficiency through quantum confinement. The GaAs-AlGaAs system is preferred in VCSEL fabrication due to the minimal lattice constant changes when the material's composition changes, allowing for the formation of multiple lattice-matched epilayers on a GaAs substrate. Additionally, the increased Al fraction affects the refractive index of AlGaAs, enabling the formation of an efficient Bragg reflector with fewer layers than other materials. At high Al concentrations, an oxide layer can form from AlGaAs, limiting the current needs in a VCSEL and allowing for a very low threshold current.

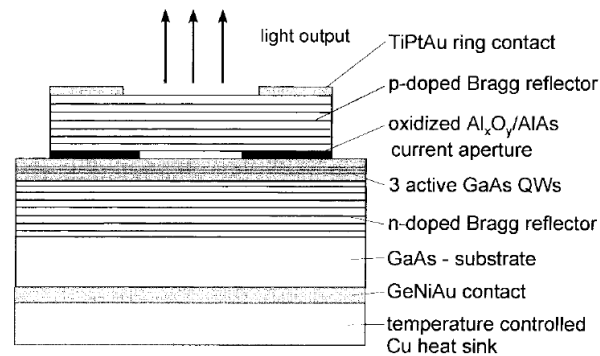


Figure 3.3: Cross-sectional view of an oxidized GaAs VCSEL (Weigl et al., 1997)

VCSELs are emerging as the top light source technology for next-generation 3D sensing and mapping applications, capable of replacing traditional laser sources such as LEDs or edge-emitting laser diodes. This is due to their vertical lasing characteristic, which makes them easier to handle during fabrication. In the fabrication process of VCSEL, a single step epitaxy process

is used where a distributed Bragg reflector (DBR) mirror is formed on the substrate. This is followed by the formation of a multiple-quantum-well (MQW) structure with current confinement, and then another layer of DBR mirror. A layer of metal contact is placed on the surface of the top layer DBR mirror to provide currents for both DBR mirrors. Millions of VCSELs can be fabricated and fully tested and analysed on a single wafer before dicing into chips, which allows for quality problems to be identified earlier and reduces fabrication costs compared to edge-emitting laser diodes.

The design and structure of individual VCSELs allow for their scalability into densely packed arrays containing tens to thousands of VCSELs on a single chip, despite their limited size (10  $\mu\text{m}$  emitting diameter) and lower output power (10 mW). This configuration, known as a VCSEL array, is suitable for high-power applications. VCSELs provide a circular light beam with lower divergence angle (about  $20^\circ$  full width at  $1/e^2$  points), making it easier to couple or collimate to an optical fiber and shape the emission pattern (Moench et al., 2019). Additionally, VCSELs can be surface mountable components (SMT), combining the features of an LED with those of a laser. Their surface emission is nearly identical to the photodetector geometry, which allows for easier alignment and assembly than edge-emitting laser diodes. The vertical output beam also makes VCSELs ideal for parallel optical interconnection and communication.

### **3.2 VCSEL for LiDAR application**

The development of VCSEL lasers has opened up a new area of laser applications, making it possible to incorporate lasers into smartphones, vehicles, households, and industries. Manufacturers of smart or automated devices are increasingly adding features to map 3D environments for identification, guidance, navigation, and augmented and virtual reality (AR/VR), and VCSELs could be the new sensors that these devices need. VCSELs provide precise data measurements of the distance to objects, thereby creating 3D visualization data and maps (Moench et al., 2018).

VCSELs are well-suited to a wide range of applications, from proximity sensing in smartphones to medium-range detection of people and objects within a few meters, as well as long-range LiDAR systems in autonomous vehicles that can determine small objects placed more than a hundred meters ahead. VCSELs are semiconductor-based lasers that offer a good quality beam, high accuracy detection, and compact size, making them an ideal laser source for 3D sensing illumination (rpmc, 2023).

In this approach, the distance is determined by analysing the time it takes for light to travel from a laser source, reflect off an object's surface, and be detected by a sensor. There are two types of TOF systems: direct (DToF) and indirect (iToF). DToF systems use laser pulses and sensitive detectors, such as single-photon avalanche diodes (SPADs), to measure the time it takes for the pulse to travel. On the other hand, iToF systems measure the phase difference

between the emitted and received pulse trains and can be found on camera chips, providing approximately QVGA lateral resolution (Moench et al., 2018).

The main limitation of the TOF technique is the interruption of photons emitted or produced by artificial light sources and the sun (Sun et al., 2016). A spectral filter is placed in front of the sensor to overcome this issue, which is centered on the laser wavelength. The narrower the laser spectrum, the narrower the bandwidth provided (Paschotta, 2008a).

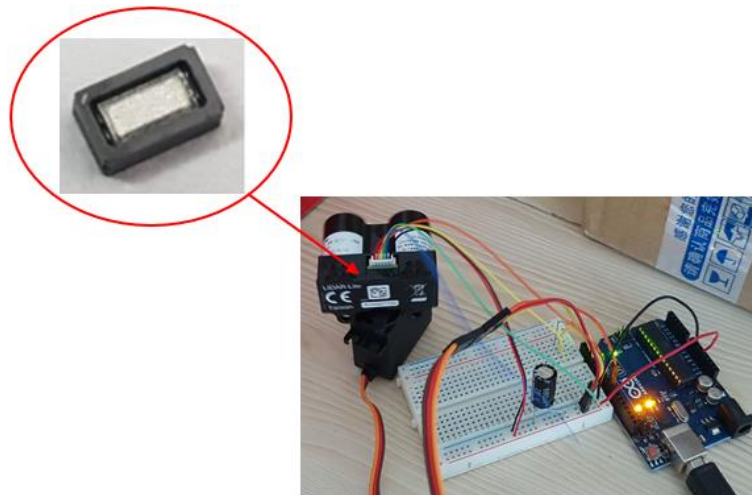


Figure 3.4: Setup of a LiDAR Sensor with scanning rotation of 180 degree

Figure 3.4 show the prototype of the testing LiDAR sensor with integrate a VCSEL as its light source. The VCSEL unit that is to be used in this LiDAR setup is PLA5506-940. From the test report, it will produce a maximum output power of 300mW when it is driven with current of 500mA (Trumpf, 2021).



### 3.3 VCSEL Laser Characterization

First, the VCSEL laser is undergoing characterization based on measurements of Power-Current and Voltage-Current.

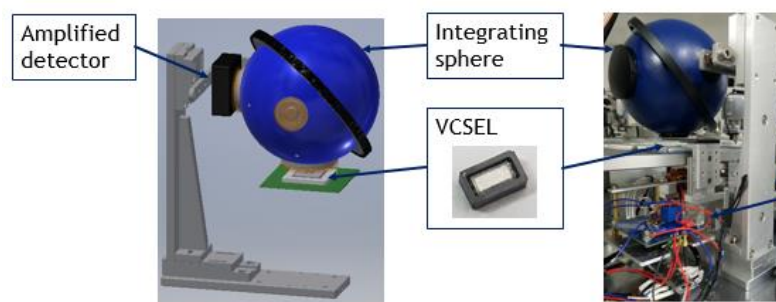


Figure 3.5: VCSEL Laser Measurement Setup

Using the setup depicted in Figure 3.5, the VCSEL laser is measured by first employing the integrating sphere for power measurement. By serving as a diffuser, the integrating sphere maintains the optical power and guides it to the detector, enabling precise measurement of the VCSEL's optical power.

In order to power up a VCSEL, a driver board is necessary to generate short electrical pulses in voltage and then convert them to current. The driver board is capable of controlling the current to produce the desired output power of the VCSEL. Current measurements were taken from 0A to 1.5A. Figures 3.6 and 3.7 illustrate the power and voltage measurements of the VCSEL laser at different currents under continuous wave (CW) conditions in room temperature. The VCSEL's threshold current is about 0.1mA at 1.5V, where an output is detected.

In Figure 3.6, the VCSEL shows a characteristic output power roll-off (indicated by the orange line) as the input current increases. This is due to the heat generated by the VCSEL as the current increases. The high temperature generated by the VCSEL causes the output power to rapidly and unstably drop as it continuously powers up. Therefore, the operating current for the VCSEL is limited to below 0.5A, resulting in a maximum output power of 0.3W.

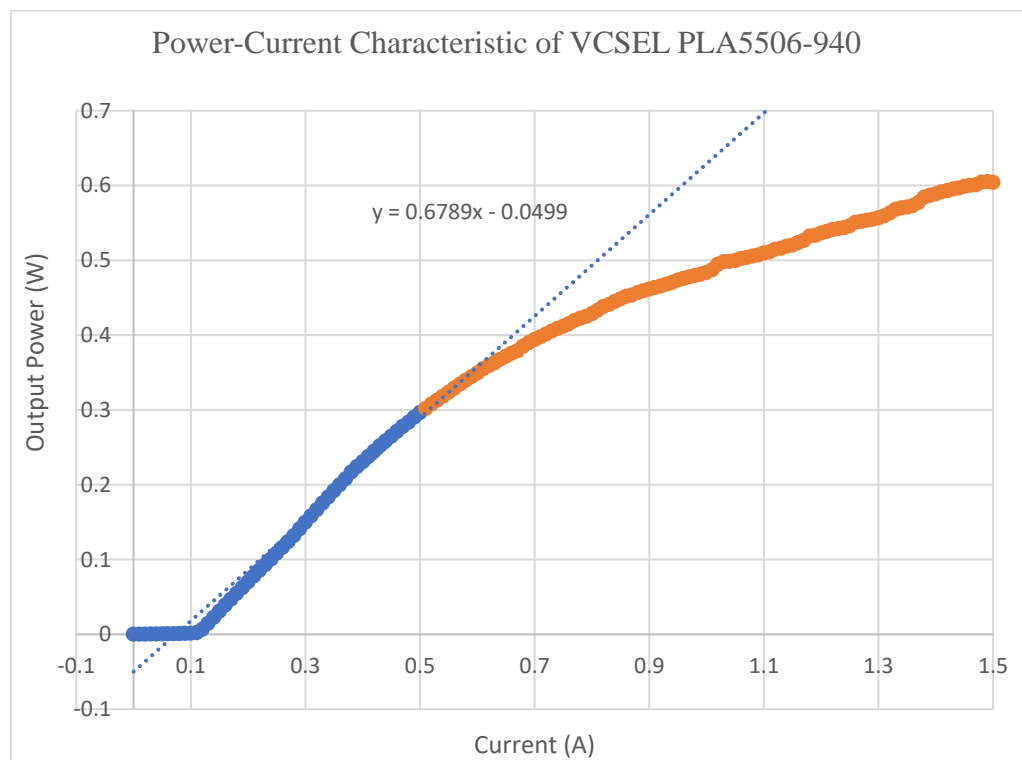


Figure 3.6: Power-Current Characteristic of VCSEL PLA5506-940

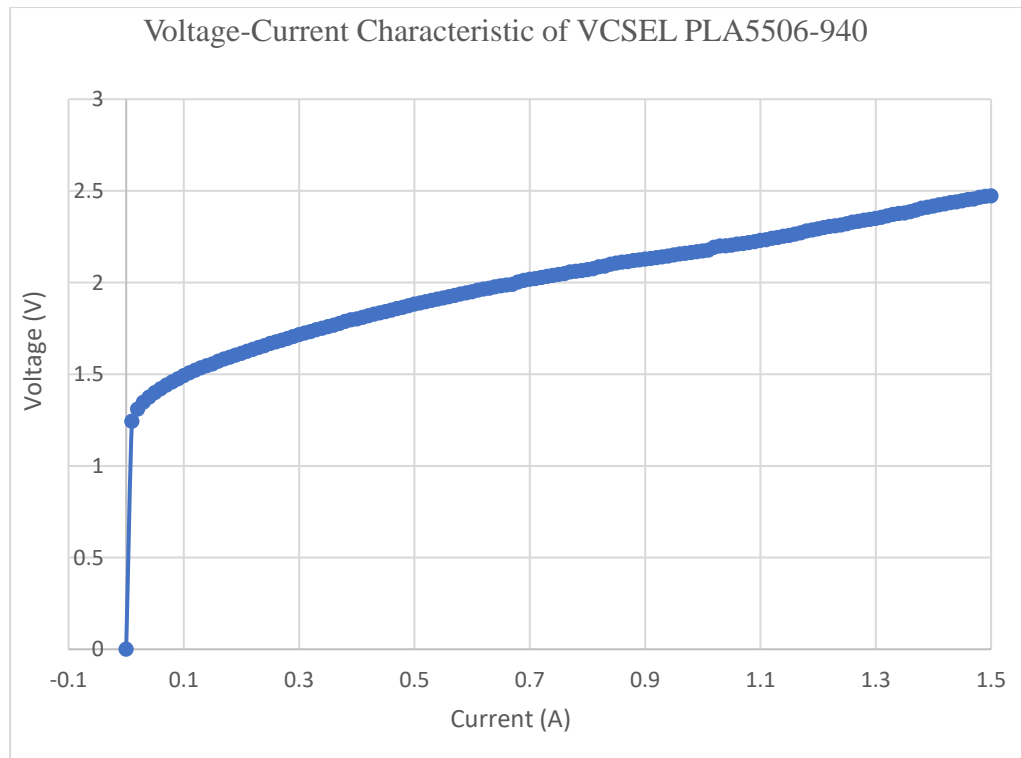


Figure 3.7: Voltage-Current Characteristic of VCSEL PLA5506-940

The oscilloscope trace of the electrical pulse from the driver and the optical pulse generated from the VCSEL is presented in Figure 3.8. However, there are bandwidth limitations to the optical pulse generated due to the limited receiver bandwidth.



Figure 3.8: Electrical Pulse and Optical Pulse Generated from VCSEL, pulse width 10us, repetition rate 100kHz.

The steep rise and fall time of the electrical pulse can be transformed into a square optical pulse at the output of the VCSEL laser. However, it is important to note that the capacitive effect on the electrical driving circuits can cause bandwidth limitations, resulting in slower rise times on the optical pulse. Despite this, a satisfactory optical pulse signal can still be achieved.

### 3.4 Implementation of VCSEL in LiDAR Setup

In this LiDAR setup, a VCSEL unit is implemented in the LiDAR Lite unit. It will be mounted to a servo motor and a stepper motor to form a 3D LiDAR configuration. In this case, the VCSEL is used as the laser light source and a photodetector in LiDAR Lite is used to receive and detect the scattered light. An Arduino microcontroller is used as a control unit to send signal in the form of pulses and to receive the returning signal from the LiDAR unit. Then, the returning signal is sent to a computer for further processing and convert it to form a data string which is then able to visualised in point cloud mapping. The Arduino microcontroller is also responsible for controlling the turning or rotation of a servo motor and stepper motor. The illustration of the entire setup is as shown in the Figure 3.9 below.

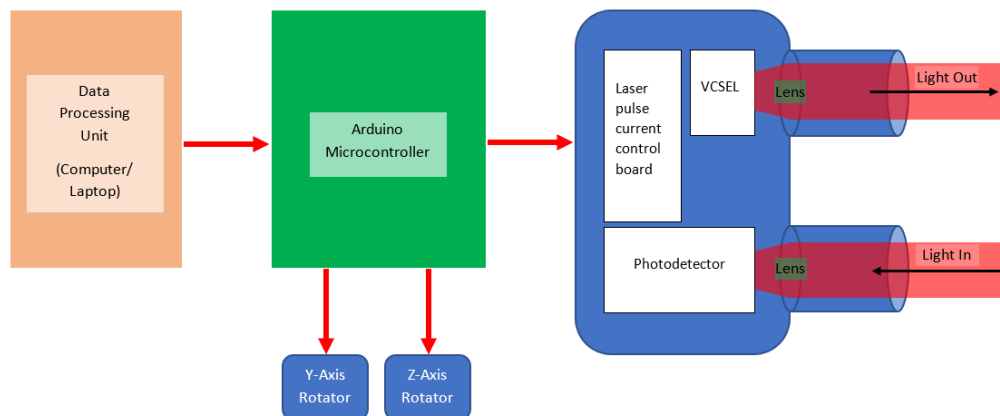


Figure 3.9: The configuration of LiDAR based on VCSEL

The Build of Material (BOM) for this experimental setup is listed in table 3.1 below.

Table 3.1 BOM list for LiDAR Setup

No	Item	Quantity
1	LiDAR Lite (VCSEL installed)	1
2	Arduino Uno microcontroller	1
3	MG995 Servo motor	1
4	Linear guide with stepper motor	1
5	A4988 stepper motor driver	1
6	100 $\mu$ F capacitor	1
7	1k $\Omega$ resistor	1
8	12V 2A power supply	1
9	DC jack	1
10	Breadboard	1
11	Jumper wires	
12	USB a to b cable	1
13	Computer / Laptop	1

Arduino Uno is an open-source microcontroller board which is the first release of USB-based Arduino board at 2010 with equipped a preprogrammed bootloader ATmega328P on the board. The board is provided with 14 digital pins and 6 analogue pins which can programmed with Arduino Integrated Development Environment (IDE) software for setting them either input or output (I/O) using an USB cable. Six of the 14 digital I/O pins able to provide

Pulse Width Modulation (PWM) output. This allowed us to control the motors in this project by providing the pulse and frequency needed. Besides, the Arduino Uno board consists a power output of 5V and 3.3V output pins by reference to the ground pin. The Arduino Uno Board can power up by connecting a supply of 7 to 20V to the DC jack or connecting a 5V USB to the USB connector (Badamasi, 2014; Arduino, 2023).



Figure 3.10: Arduino Uno Microcontroller (Arduino, 2023)

The following section will discuss on the construction of 3D scanning LiDAR, step by step from a simple setup of fixed distance measurement LiDAR to a rotating LiDAR with scanning range of 180-degree and lastly a 3D scanning LiDAR which is able to collect data in the form of x, y and z coordinates.

### 3.4.1 Measurement of Distance

With the characterization work done on VCSEL as a laser source in section 3.3, the next step is to characterize the LiDAR performance in terms of a single point distance measurement. The device is modified by using a VCSEL unit as the light source and the receiver module of the LiDAR Lite, a commercially available unit and placed in front of a target. The LiDAR device is connected to an Arduino microcontroller using PWM mode for signal data transfer. The returned signal from the LiDAR will be transferred to the Arduino microcontroller for processing before transferring to PC via a USB connection. The Figure 3.11 below shows the distance measurement setup of the LiDAR sensor and Arduino UNO to a surface of an object.

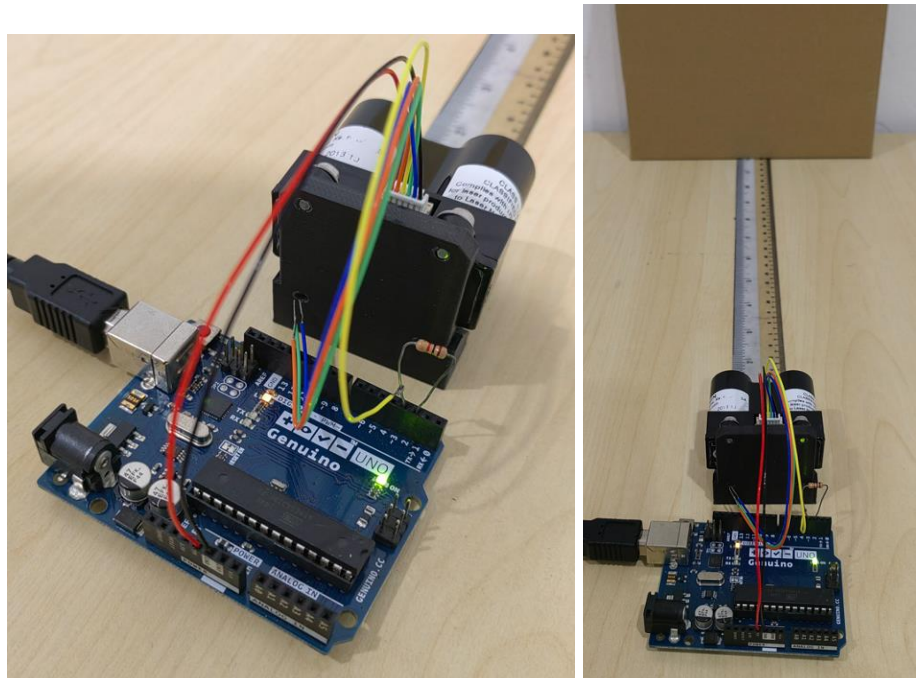


Figure 3.11: Setup of VCSEL integrate into receiver module of the LiDAR Lite for distance measurement.



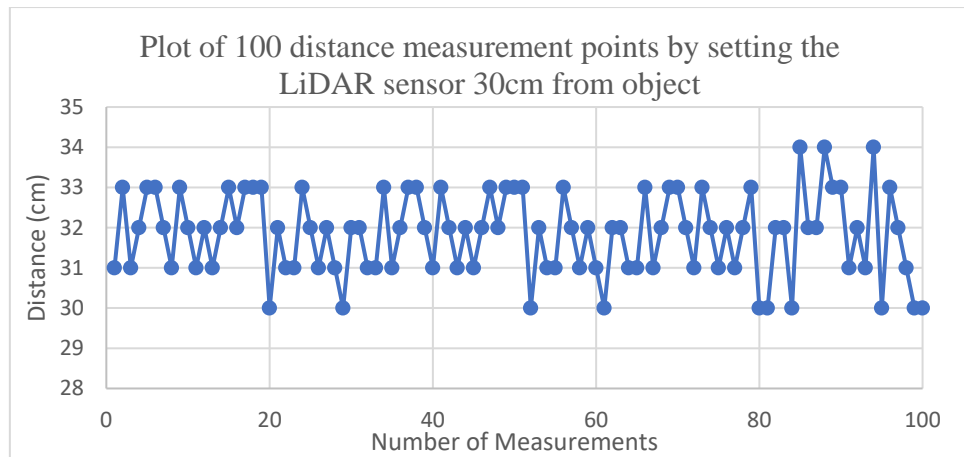


Figure 3.12: Graph of collecting 100 measurements by fixed the distance of LiDAR at 30cm from surface of an object

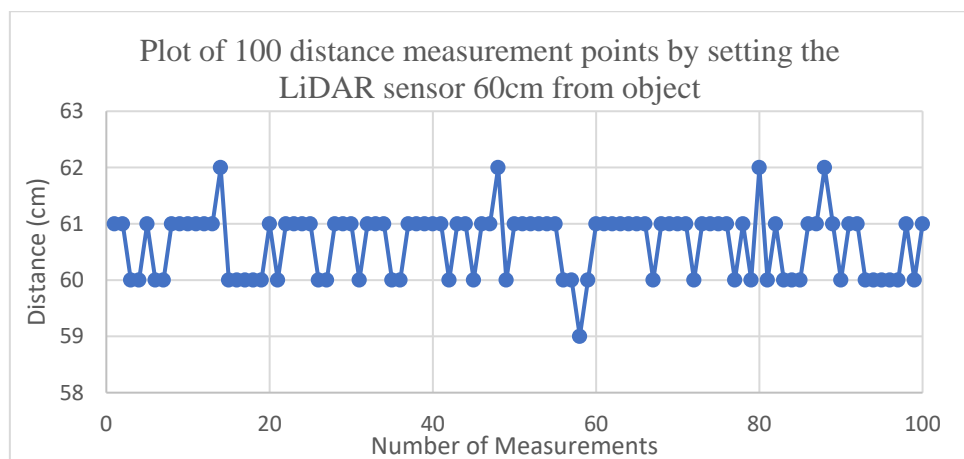


Figure 3.13: Graph of collecting 100 measurements by fixed the distance of LiDAR at 60cm from surface of an object

Figure 3.12 and 3.13 shows two sets of data which collecting 100 measurements continuously by setting the position of LiDAR sensor at different distance, 30cm and 60cm from an object. From the graph plot, we can observe that the LiDAR sensor able to measure at more stable condition by placing it at further distance to an object although it has an error of  $\pm 2$ cm.

### 3.4.2 Data Collection for a Single Plane

Then, the LiDAR device is mounted on a servo motor for measuring the distance of a surface at every degree the servo motor turns. The device will receive the distance measurement readings continuously as it is rotated (0-180 degrees). In this case, we have both the distance measurement and rotation angle data at every degree rotation.

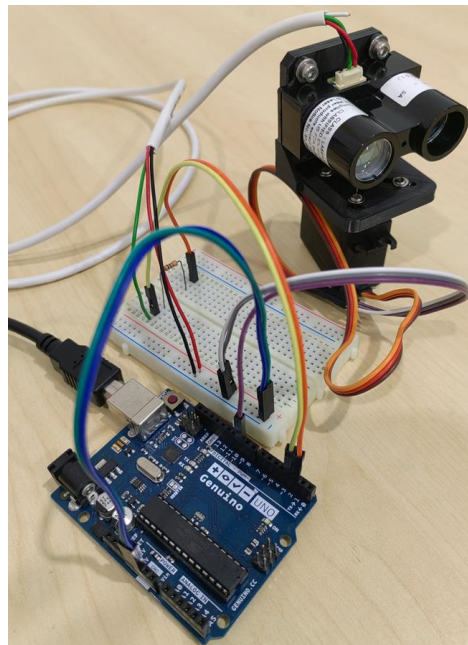


Figure 3.14: Setup of LiDAR unit mount on servo motor.

Unfortunately, the measurement recorded in angles or polar form is unable to support and understand by most software. Thus, the data needs to be converted to cartesian form or in this case the XY coordinates. Figure 3.15 shows the setup of the LiDAR to scan a space build by using pallet woods and Figure 3.16 shows the plot of measurement data in graph.



Figure 3.15: Scanning of LiDAR rotate 180-degree with servo motor

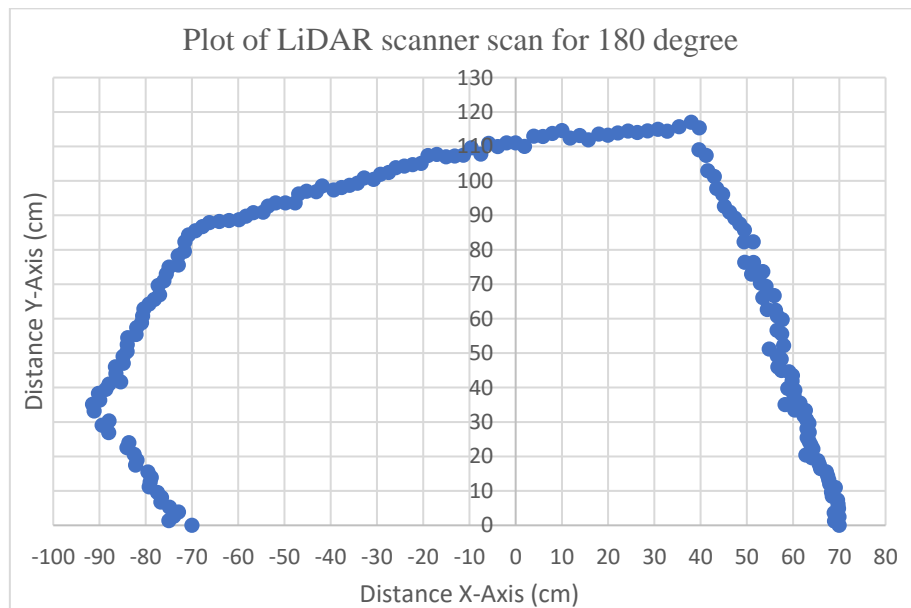


Figure 3.16: Plot of scanning LiDAR turning 180-degree in the platform build by pallet woods.

The result in Figure 3.16 is done with an averaging of 10 points. From the plot, it resembles the shape of the inner pallet woods. The average value of 10 was selected as it gives the best measurement and the shortest acquisition time.

### 3.4.3 Setup for a 3-dimension Scanning (3D) LiDAR

In order to achieve 3D measurement, additional axis in the z-direction has to be added in the current LiDAR setup. This is done by mounting it on a linear slider with stepper motor that will move the LiDAR device in z- direction (up and down). The continuous measurement of distance from LiDAR to the surfaces at different scanning angles (180-degree rotation by the servo motor), and the vertical data collected will provide a map of point clouds of the environment. The setup is as shown in Figure 3.17 below.



Figure 3.17: Setup of a 3D LiDAR with 3D printed holder.

In Figure 3.18, the LiDAR Lite (modified with VCSEL as light source) was mounted on a 3D printed frame, while the MG995 servo motor was also mounted onto the frame with the LiDAR sensor attached to its rotor. Then, another 3D printed bracket is used to connect between the servo motor and the linear slider. Lastly, a 3D printed base is printed to hold the linear slider stand vertically.

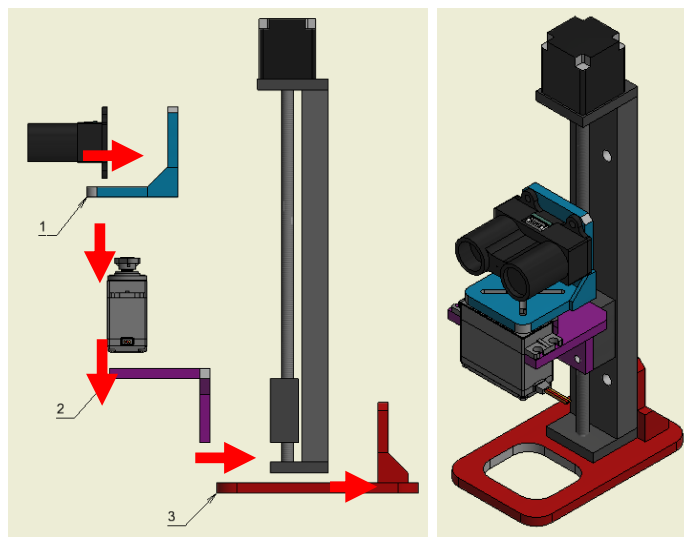


Figure 3.18: 3D model for the LiDAR setup

Figure 3.19 illustrate the connection between the components. The LiDAR unit is power up with 5V and GND pin and the signal is controlled by the PWM mode pin. The PWM mode pin of the LiDAR unit is connected to one side of 1k $\Omega$  resistor and the same side is connected to pin 3 of Arduino uno as the monitor pin for detecting the returned signal triggered by the trigger pin which is pin 2 of the Arduino uno (connect by the other side of 1k $\Omega$  resistor). The MG955 servo motor also have three pin terminals which are signal, power and ground pins. The signal pin is connected to pin 10 (as PWM output) of the Arduino uno and the power and ground pins is connected to 5V and GND pins of the Arduino uno.

Then, the linear slider stepper motor needs a stepper motor driver and external power supply to activate. An A4988 stepper motor driver is used. The Arduino uno pin 8 and pin 9 is connected to the DIR and STEP pin of the stepper motor driver. The DIR pin is used to control direction of the stepper motor by setting the pin either high or low, while the STEP pin is used to control the turning steps of the stepper motor. In our case, the STEP pin is receiving a number of pulses to control the moving distance of the slider block. The more pulses are applied to the STEP pin the longer the moving distance.

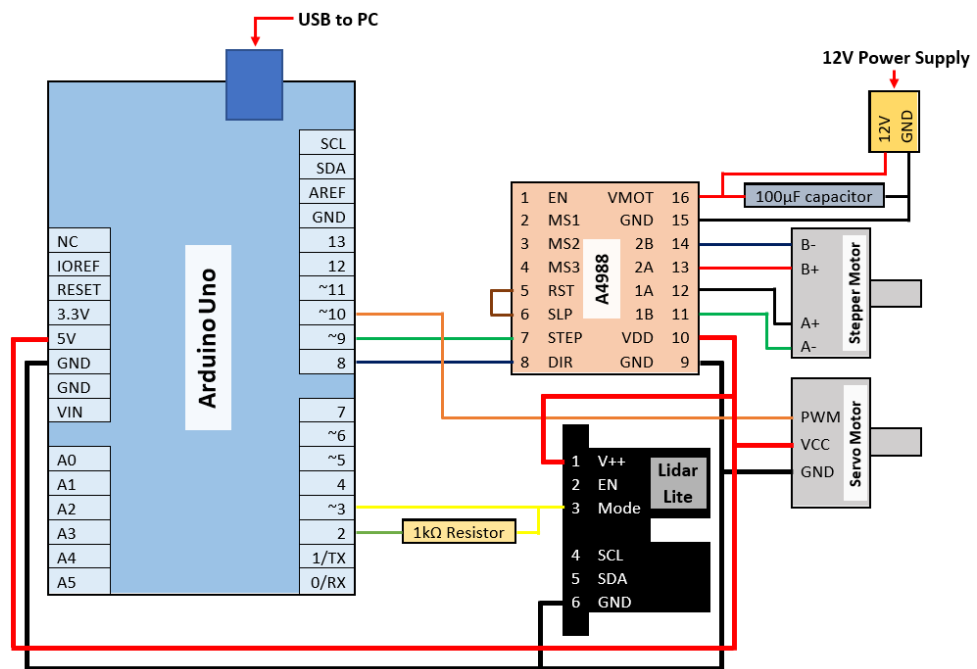


Figure 3.19: Connections of the components

The overall dimension of the system is approximately 70mm in width, 100mm in length and 220mm in height. The volume of the designed LiDAR system is 2135% smaller than Velodyne HDL-64E mechanical LiDAR. The results from the scanning LiDAR can be plotted on the LiDAR visualizer. This will be discussed in detail in Chapter 4.

## CHAPTER 4

### LIDAR SOFTWARE AND IMAGING

Point cloud is a type of 3D data representation that consists of a large number of points in 3D space. Each point in the point cloud represents a specific location in space and is defined by its x, y, and z coordinates. The points can be of different sizes and colours, and they can be organized in a variety of ways, such as in a grid or in a more unstructured pattern. Point clouds are often used in applications such as 3D modelling, surveying, and robotics. They are particularly useful in situations where a high level of accuracy and detail is required. For example, point clouds can be used to create 3D models of buildings, bridges, and other structures, allowing architects, engineers, and construction workers to better understand the layout and dimensions of these objects. Figure 4.1 shows an example point cloud of an environment.

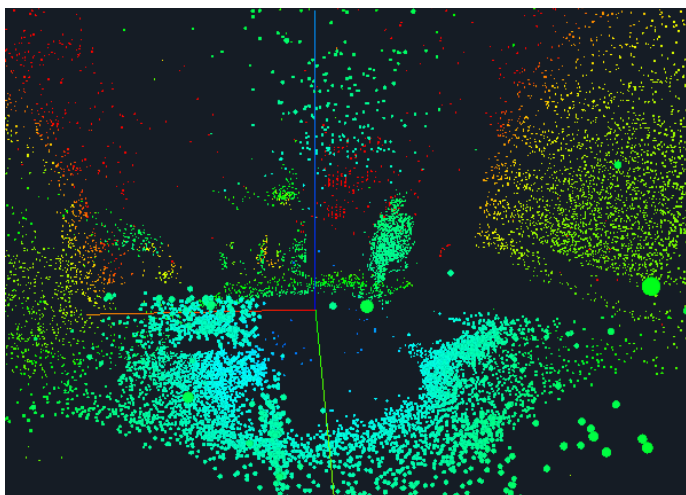


Figure 4.1: Point cloud of an environment (Ng, Lim and Teh, 2020)

One of the advantages of point clouds is that they can be easily captured using a variety of sensors, such as LiDAR or photogrammetry systems. These sensors emit light or take photographs to capture data about the environment, and the resulting data can be processed to generate a point cloud. The accuracy and level of detail of the point cloud depend on the resolution of the sensor and the quality of the data processing algorithms.

To visualize and analyse point clouds, specialized software is often used. This software can help to manipulate and filter the point cloud data, as well as generate visualizations that make it easier to understand and interpret the data. In this chapter, there are three main components discussed that can be combined to collect, convert and visualise the point cloud data measured by using the modified LiDAR hardware which discussed in the previous chapter, chapter 3.

The first component is the sketch for the Arduino Uno microcontroller, which is used to control the LiDAR hardware and collect data from sensors. The Arduino Uno is a popular microcontroller board that is often used in projects that involve collecting and analysing data. A sketch is created to provide a program that can be uploaded to the microcontroller to gather data from the LiDAR sensor. The collected data is then stored in a text file which can be processed further.



The second component is a conversion tool that can be used to convert the text file to .pcd file format. The .pcd format is commonly used for point cloud data and is supported by many visualization tools. The conversion tool takes the text file as input and generates a .pcd file that can be used for further analysis and visualization.

The third component is a visualizing tool that can be used to show the point cloud. The visualizing tool takes the .pcd file as input and generates a visual representation of the data. This tool helps to analyse the data and identify any patterns or trends that may be present.

In combination, these three components provide a complete solution for collecting, converting and visualizing of point cloud data. This process can be applied to a wide range of projects and applications, from environmental monitoring to industrial automation. By using the Arduino Uno microcontroller, a conversion tool and a visualizing tool, it is possible to collect and analyse data in a variety of settings and draw insights that can inform decision-making.

## 4.1 Collection of Point Cloud Data

The idea of the project is to construct a system that is compatible to the modified LiDAR hardware and able to perform basic point cloud visualization using PCL. The collection of point cloud data is needed. A laptop was used to process the data collected from the LiDAR hardware. The laptop was connected to the Arduino microcontroller. The LiDAR unit was mounted on the 3D printed frame, as show in Figure 3.18 and attached with servo and stepper motor are connected to the Arduino microcontroller. Figure 4.2 shows the illustration of the interface between the components.

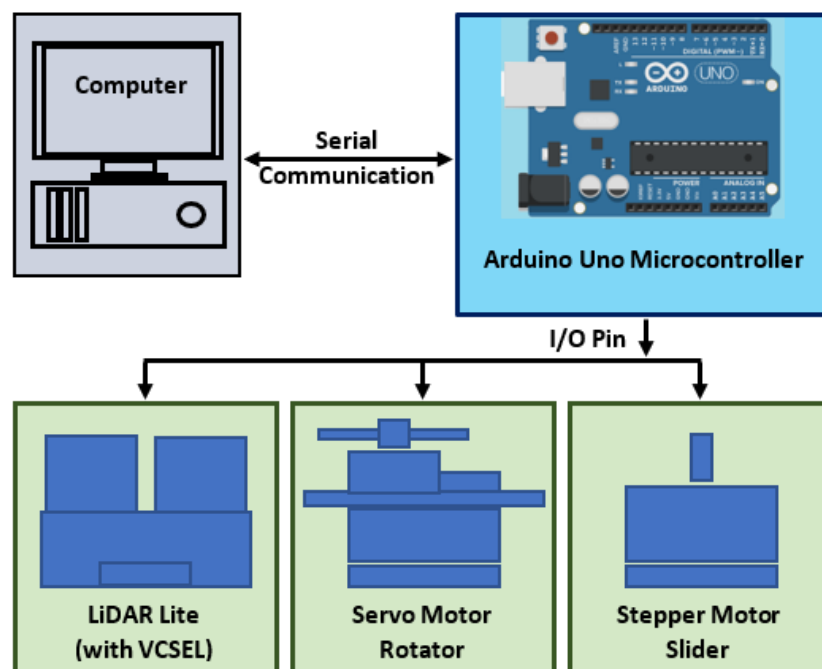


Figure 4.2: Illustration of the interface between the components

There are three main steps involved for the raw point cloud data collection. First, the signal pin from the microcontroller is triggered, which sends out a signal to the LiDAR sensor. Second, the microcontroller calculates the time it takes for the return signal to be detected by the sensor. This time calculation is based on the principle of TOF, which measures the time it takes for a signal to travel to an object and back. Finally, the received signal is converted to distance, using a simple formula that takes into account the speed of the signal and the time it took to travel to and from the object. This distance data is collected, arranged and recorded in a text file.

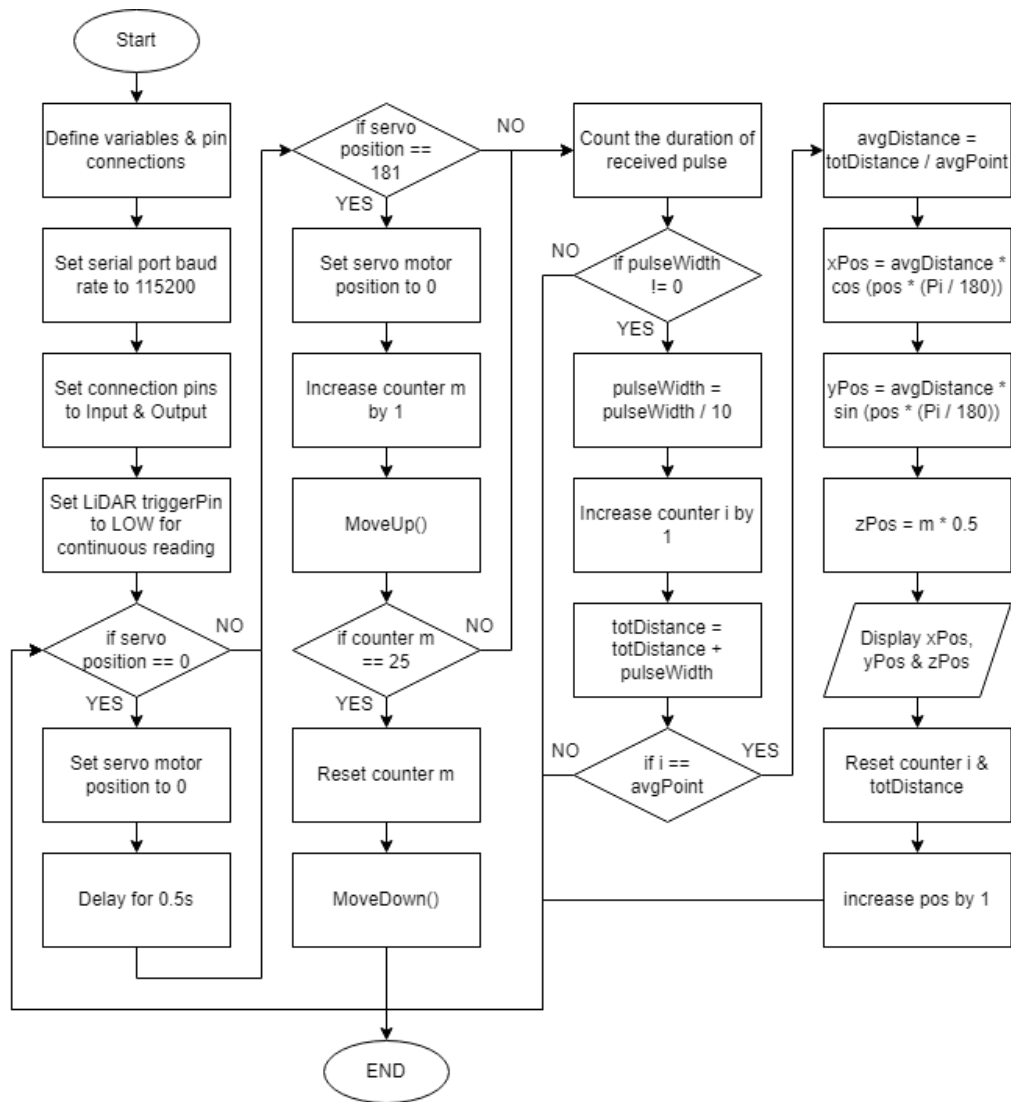


Figure 4.3: Flow Chart of Arduino sketch to perform 3D scanning

Figure 4.3 show the overall flow chart of Arduino sketch collecting point cloud data. The sketch starts with defining variables and pins that will be used in the program. This is important because it tells the program which pins on the microcontroller are connected to the LiDAR sensor, servo, and stepper motor. Without this information, the program wouldn't know how to communicate with these components. Next, the program sets the serial port baud rate to 115200. This is the rate at which data is transmitted between the microcontroller and the computer. It's important to set this rate correctly so that the program can

effectively communicate with the computer. Then, the connection pins are defined to be either input or output. The purpose of this setting is to determine which pins are used for sending and receiving signals between the microcontroller and other components. After all of the connections were completely defined, the sensor trigger pin was set to low, which means that it will continuously read data from the sensor. This ensures that the program is constantly receiving data from the sensor. Before the LiDAR starts scanning and recording the measurement, the servo motor position is checked to ensure it is at position 0. If it is, the program proceeds to the next step. If it isn't, the program will turn the servo motor to position 0. This is important because it ensures that the program starts taking measurements from a known position. Once the servo is at position 0, the program will count the duration of the pulse it receives from the LiDAR sensor. At the same position, 10 measurement data points are recorded and added up, and their average is calculated. The averaging of the data is performed to ensure that the program is receiving accurate and consistent data from the sensor. The averaging will be performed on each degree the servo motor turns. This allows the program to take measurements at every angle it turns and create a more detailed map of the surrounding environment. When the servo reaches 180 degrees, it will return to 0. This allows the program to take measurements in a complete 180-degree sweep. Then the stepper slider will move up and continue scanning of the other plane. The steps will repeat until the slider reaches the maximum distance and will reset and move down to the original position.

### 4.1.1 Data Conversion from Polar to Cartesian Form

At the beginning, the data was recorded in polar form which is the distance and angles. However, to represent and process the data in most applications, it is usually more convenient to convert the polar coordinates to Cartesian coordinates. This is because most algorithms and software packages for processing 3D point clouds are designed to work with Cartesian coordinates. To convert from polar to Cartesian coordinates, the distance and angle measurements for each point in the point cloud are used to calculate the x, y, and z coordinates of the point relative to the origin of the LiDAR scanner. This results in a set of 3D points that can be used to create a high-resolution 3D map of the scanned environment, or to perform other types of analyses and processing.

In the LiDAR setup proposed, there are just 2 components needed to convert from polar coordinate to cartesian form, which is x coordinate and y coordinate, as the z position for the setup is set to move by a constant distance, 5mm. The distance measured by the LiDAR sensor represented as  $r$  and the turning angle of the servo motor represented as  $\theta$ . The conversion is as Figure 4.4 below.

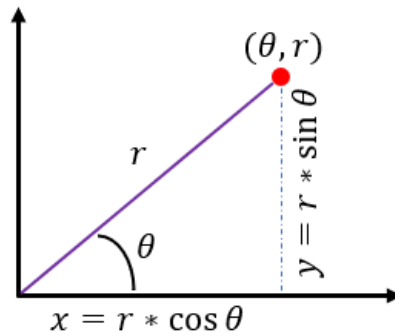


Figure 4.4: Conversion of polar form to cartesian form

#### 4.1.2 Arrangement of Data

Every measurement data and angles are arranged and recorded in a text file. The arrangement is as Figure 4.5 below:

```

70.00 0.00 0
68.99 1.20 0
69.96 2.44 0
68.91 3.61 0
69.83 4.88 0
69.73 6.10 0
69.62 7.32 0
68.49 8.41 0
68.33 9.60 0
69.14 10.95 0

```

Figure 4.5: 10 Sample of LiDAR raw data recorded

The first column is X coordinate data. The second column is Y coordinate data. The last column is Z coordinate data. All recorded data is in cm. The data is arranged by its category and separated by a space delimiter. The delimiter is used to separate or mark the boundaries between different pieces of data. This is important to allow the conversion tools, which will describe in next part to parse and extract the individual pieces of data within the file, and to manipulate or process them.

### 4.1.3 Averaging of Data

An average is calculated for each degree that the servo turns. This is to increase the precision and accuracy of data by reducing the effect of outliers or extreme values that may skew the overall results. By smoothing out the fluctuations and reducing the impact of individual measurement errors, averaging can provide a more accurate and consistent estimate of the map of the surrounding environment. Figure 4.6 below is the environment built to scan and analyse the point cloud data.



Figure 4.6: Testing of 3D LiDAR scanning

Figure 4.7 and 4.8 shows the point cloud data of scanning a single plane, one complete servo rotation, 180°; while, Figure 4.9 and 4.10 shows the top view 3D point cloud of a scanned environment. By comparing the figures, it is very obvious to see that the point cloud of performing averaging of 10 measurement is look tidier and closer to the actual environment. The point cloud without performing averaging have some extreme values that makes the point cloud noisy and irregular. The outliers and extreme value will make the point cloud is challenging to identify patterns and relationships.





Figure 4.7: Top view of point cloud scanning a single plane without performing averaging



Figure 4.8: Top view of point cloud scanning a single plane with performing averaging of 10 measurements

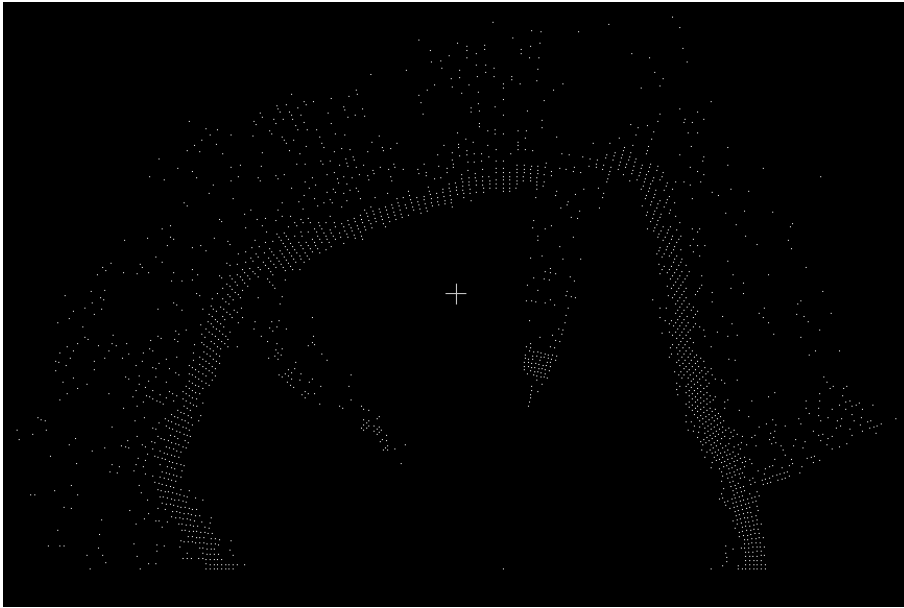


Figure 4.9: Top view of 3D Point Cloud scanning without performing averaging

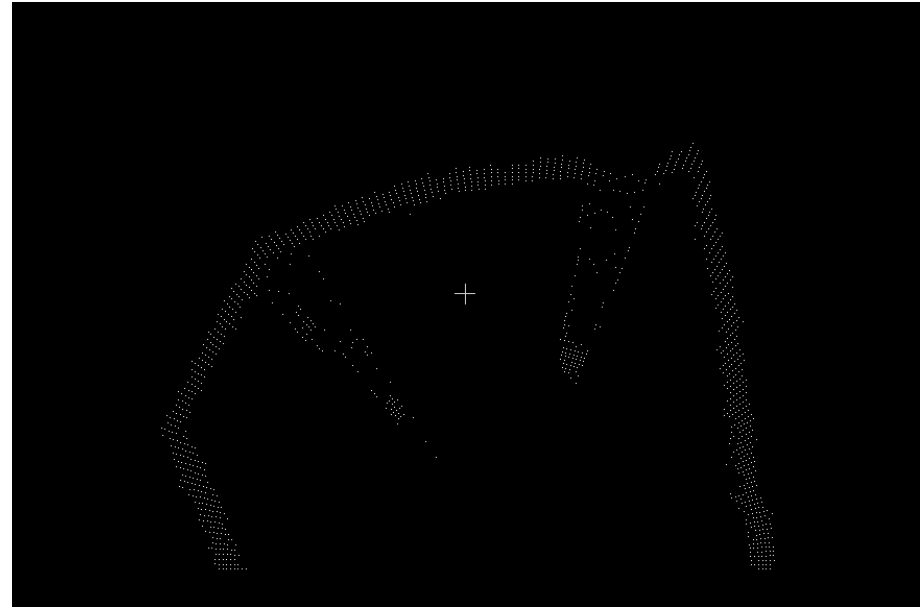


Figure 4.10: Top view of 3D point cloud scanning with performing averaging of 10 measurements

#### 4.1.4 Measurement Speed

The time to complete a measurement is depends on the averaging points. The more the points of averaging, the longer the time taken to complete a scanning.

Table 4.1 below shows the time taken to complete the scanning with and without performing the averaging of a single plane.

Table 4.1: The time taken for completing a single plane scanning with and without performing averaging.

Points of averaging	Time taken to complete a scanning, s
0	6
5	21
10	41
15	61
20	81
25	100
30	121

#### 4.1.5 Accuracy of the LiDAR Scanner

LiDAR is a remote sensing technology that uses laser light to measure distances to objects. Investigating LiDAR measurements could involve understanding the principles behind how LiDAR works, its applications, and its limitations. To conduct a controlled measurement, it would be necessary to build an area or target. In this research, the target was made of a wood-based material. This involved constructing a panel or structure using wood panels. The panel or structure would then be used as the target for the LiDAR measurements. Figure 4.11 shows the constructed structure of the wood panels.

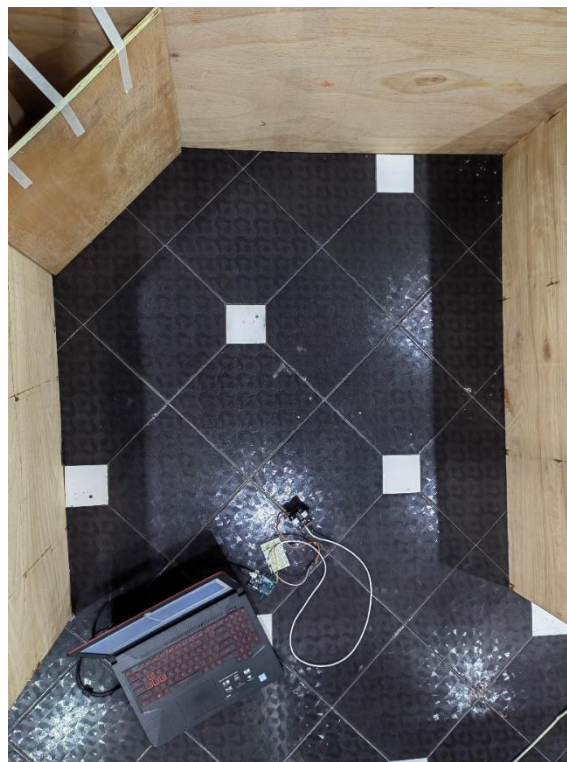


Figure 4.11: Setup and actual dimensions for measurement of point cloud

One of the principles behind how LiDAR works is TOF. TOF is a method of determining the distance between an object and the LiDAR sensor by measuring the time it takes for a laser pulse to travel from the sensor to the object and back. The laser pulse is emitted by the LiDAR sensor and bounces off the object, and the time it takes for the pulse to return to the sensor is measured. Since the speed of light is constant, the distance between the LiDAR sensor and the object can be calculated based on the time it takes for the laser pulse to travel to the object and back, using the following formula:

$$Distance, d = \frac{Speed\ of\ light \times Time\ of\ flight}{2}$$

where the speed of light is approximately  $3 \times 10^8\ m/s$ , and the Time of flight is the time taken for the laser pulse to travel from the LiDAR sensor to the object and back. This is the basic principle behind TOF-based LiDAR measurements.

To ensure accurate measurements, the light source used in LiDAR systems must be carefully calibrated. For example, if the laser pulse width is too long, the LiDAR will have reduced range resolution, while if the pulse width is too short, the LiDAR will have reduced signal-to-noise ratio. Therefore, the LiDAR system used VCSEL laser is calibrated with pulse widths of  $10\ \mu s/cm$ , which enables to achieve high-resolution and high-accuracy measurements over long ranges.

The point cloud in Figure 4.12 below shows the shape and boundary of the structure clearly. However, it is difficult to determine the exact dimensions from the image alone. Therefore, a more detailed analysis is necessary to accurately measure the dimensions of the structure.

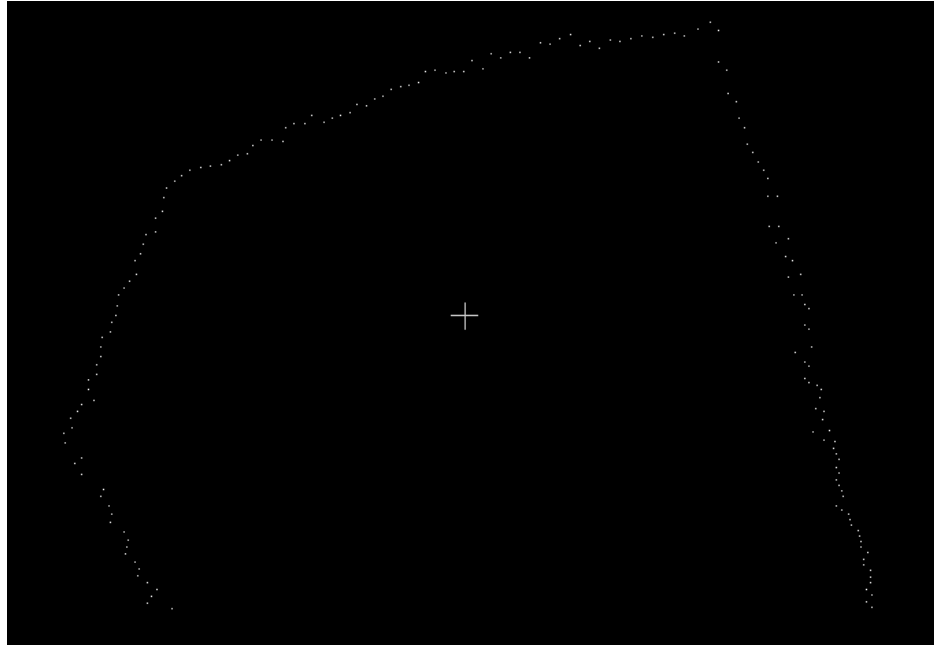


Figure 4.12: Point Cloud of the controlled measurement structure

The analysis can be performed using the edge points, which are easily identifiable on the graph. The edge points and the distances needed to determine them are labelled on Figure 4.13. To calculate the distance between two points on the graph, the following formula can be used:

$$\text{Distance, } d = \sqrt{(x_2 - x_1)^2 + (y_2 - y_1)^2}$$

where  $(x_1, y_1)$  and  $(x_2, y_2)$  are the coordinates of the two points being measured. By using this formula and the known scale of the graph, the dimensions of the structure can be accurately determined.

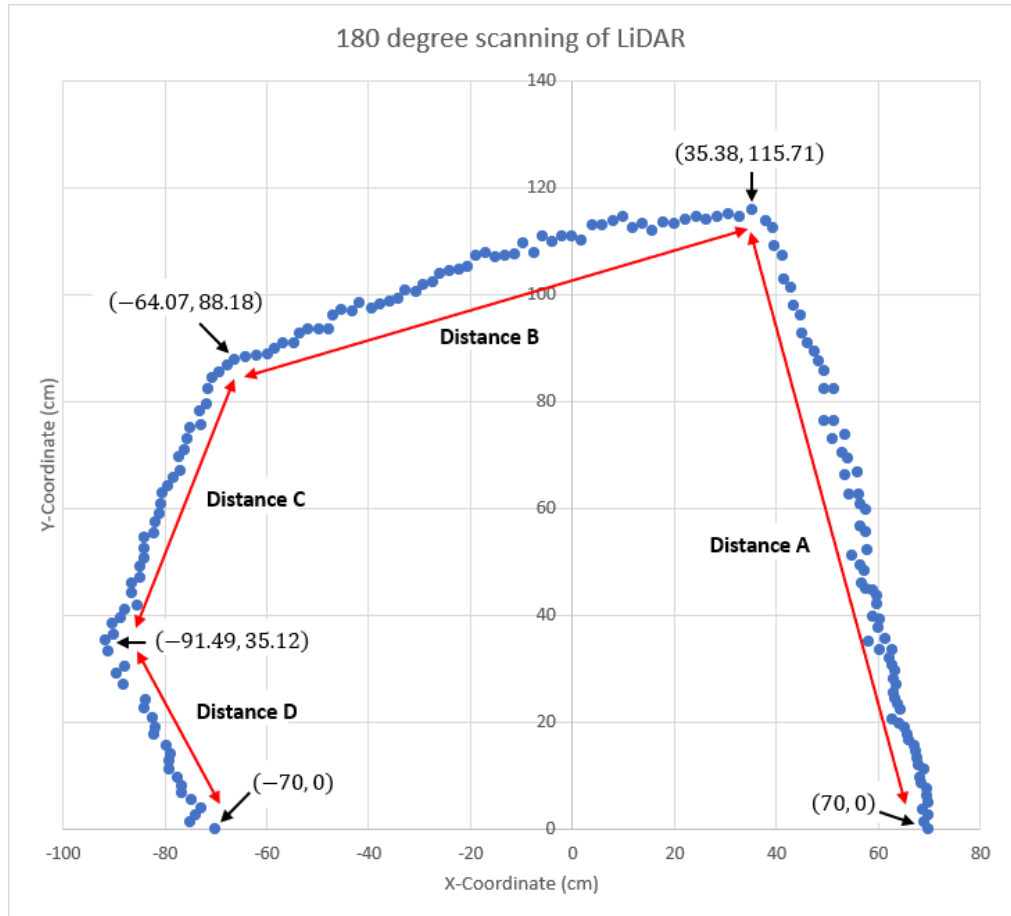


Figure 4.13: Measurement of the controlled structure

Table 4.2: Comparison of controlled structure dimension of actual structure and point cloud measurement

	Actual Structure	Measurement from Point Cloud
Dimensions	<p>Distance B = 84cm Distance C = 50cm Distance A = 100cm Distance D = 65cm 180° 0° LiDAR Scanner</p>	<p>Distance B = 103.02cm Distance C = 60.29cm Distance A = 120.78cm Distance D = 41.17cm 180° 0° LiDAR Scanner</p>
Area	11782.5cm <sup>2</sup>	12952.3cm <sup>2</sup>



According to Table 4.2, the distance and the area of the actual structure and the point cloud measurement is calculated. The measurements for distance A and distance D were ignored for the comparison due to about 10-degree tilt of the LiDAR sensor and affect the measurement. By comparing the measurements for distance B and distance C, the distance measured by the LiDAR sensor for the point cloud was longer than the actual measured distance. However, the 10-degree tilt of the LiDAR sensor will not affect the area calculation. The area calculated shows the measurement from the point cloud is bigger and have a percentage different of 9.93% compared to the actual structure. There are two possible causes for this occurrence. Firstly, this could be due to the presence of wood surfaces, which can affect LiDAR measurements. Wood surfaces can cause errors in LiDAR measurements as they can absorb, reflect, and scatter laser pulses. The amount of energy absorbed or reflected by the wood surface depends on several factors, including the type of wood, its surface condition, density, and moisture content (Sandak and Tanaka, 2003; Rose, 2018; Besseau et al., 2020). This can result in incorrect distance measurements or incomplete data capture, leading to potential errors in the resulting point cloud. Secondly, the error may be caused by the averaging calculation of the measurements. Some of the outliers and extreme values are farther than the actual distance, and they are included in the average value, causing the point distance to increase.

## 4.2 Point Cloud Data Conversion

Compatibility is always the main challenge when ensuring that a processing system accepts correct input data. Some of the point cloud data formats recorded in azimuth are not supported by most software. Therefore, a converter is needed for visualization software that can process several file formats. The converter must be capable of processing multiple file formats to provide flexibility for users, and it should be designed to perform conversions in a simple, intuitive manner that doesn't confuse the user. This is particularly important because users may be unfamiliar with different file formats and may not have technical expertise. Therefore, the converter should be user-friendly and have a simple interface. In addition to converting files, the converter should also have the flexibility to accept files recorded in either cartesian or polar coordinates. This will enable users to work with a wide range of point cloud data, regardless of how it was originally recorded. Once the software is designed, a dataset can be created and analysed using the software's visualization tools.

### 4.2.1 Conversion tool program flow

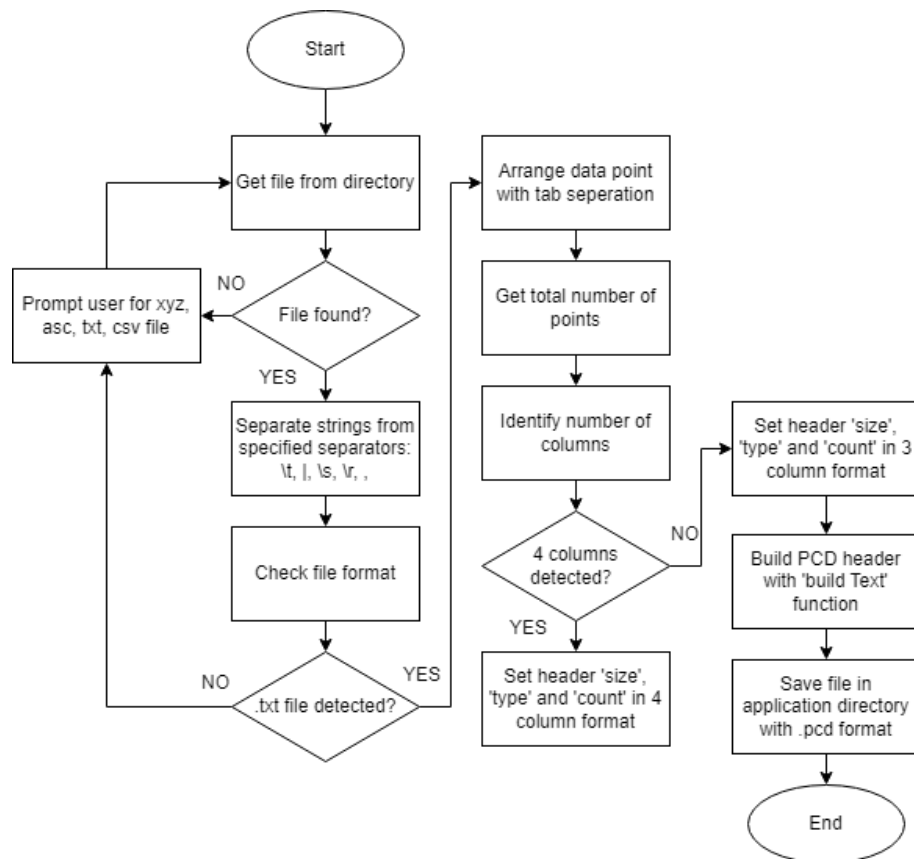


Figure 4.14: Flow chart of conversion .txt file to .pcd file

Figure 4.14 shows the flow chart of the conversion program designed for converting data from a text file. The user is prompted to input a .txt file, which the program then processes and converts to .pcd format. At the start of the application, it will retrieve the input file from a designated directory. If the file is not found, the application will filter for error code and prompt the user to provide the necessary input. The program will then read strings from the input file using I/O functions and separate them by comparing with a pre-defined array of separators (e.g., '\t', '|', '\s', '\r', and ','). The code will check if the input file is in .txt format, and if true, it will detect the number of points and columns

in the file. Depending on the number of columns detected (3 or 4), the program will build the header type 'size', 'type', and count accordingly. Lastly, the program will save the file in .pcd format.

#### 4.2.2 User Interface Operating Flow

The conversion tool aims to simplify the conversion process and prevent confusion for users. To convert a .txt file to a .pcd file, the following steps are required:

1. Locate the directory of the .txt file.
2. Optionally, select the checkbox to indicate whether cartesian to polar conversion is required.
3. Click the 'Convert' button.
4. Check the converted .pcd file in the application directory by opening it with Notepad.

By following these steps, users can easily convert the .txt files to .pcd files without any confusion.



Figure 4.15: User interface of PCD conversion tool

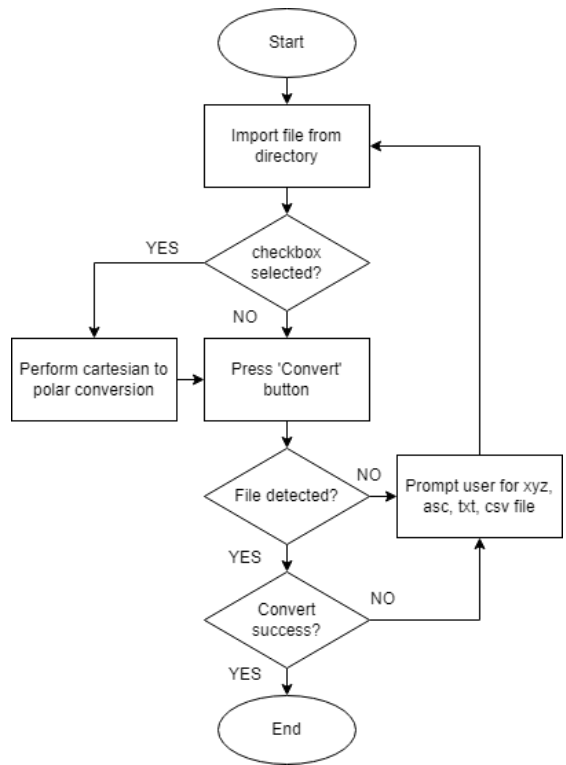


Figure 4.16: User interface design flow for PCD conversion tool

### 4.2.3 PCD Conversion Results

When working with data in a .txt file format, it is important to ensure that the data is separated correctly to allow for easy analysis and processing. In this regard, a space-delimited format is used. The converter will identify separator according to matching characters, in this case ‘\s’ is matched, where each data point is separated by a space. To convert this format into a .pcd file, the converter will automatically identify the separator and separate the data accordingly. Once the data has been identified, it can be used directly to build the header for the .pcd file by using the number of points and columns.

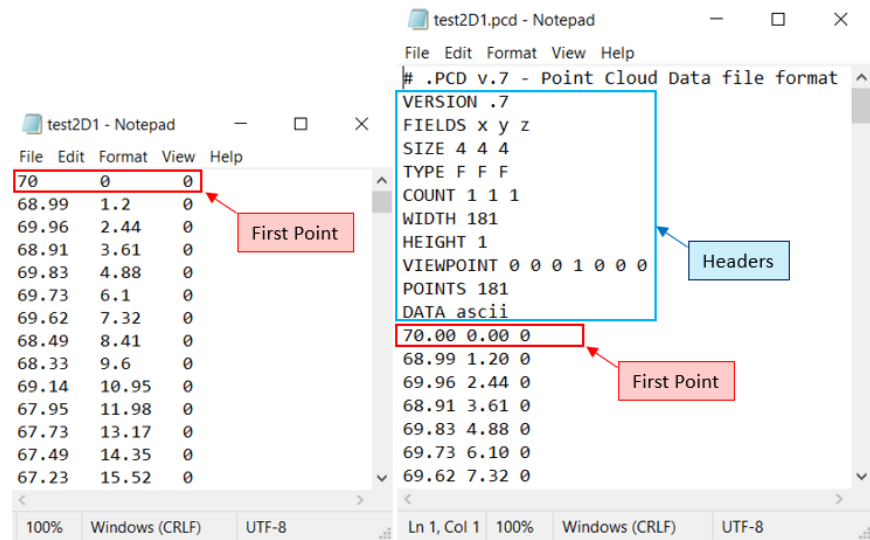


Figure 4.17: Conversion from .txt file (left) to .pcd file (right)

From the conversion, the header of a .pcd file is created. The definition of the created header is described in the Table 4.3 below:

Table 4.3: Header description for the converted .pcd file

Header Field	Description
VERSION	The version of the Point Cloud Library used is version 0.7
FIELDS	The data is listed in 'x', 'y' and 'z', which represent the 3D spatial coordinates of each point
SIZE	The size of each field in a row is 4-byte long, the size would be $4 * 3 = 12$ bytes
TYPE	The data type for each field is float type, F
COUNT	The number of elements in each field. x, y, and z would each have a single instance count of 1.
WIDTH	The number of rows of the data is 181.
HEIGHT	It is set to 1. each point in the file is represented as a one-dimensional array
VIEWPOINT	The default value of viewpoint is set.
POINTS	The total number of points in the file is 181. (WIDTH *HEIGHT)
DATA	The data type of the point cloud data is stored as ASCII

### 4.3 Visualisation of Point Clouds

A Windows Forms application was developed using the C# programming language. This program allows users to load and display point clouds in PCD or XYZ format. There are two viewing options: a 2D mode with image overlay and a 3D mode that offers complete rotation of the point cloud. The program uses the Point3D class to represent individual points in 3D space, with each point defined by its X, Y, and Z coordinates. This application can be a useful tool for visualizing a complex 3D data set.

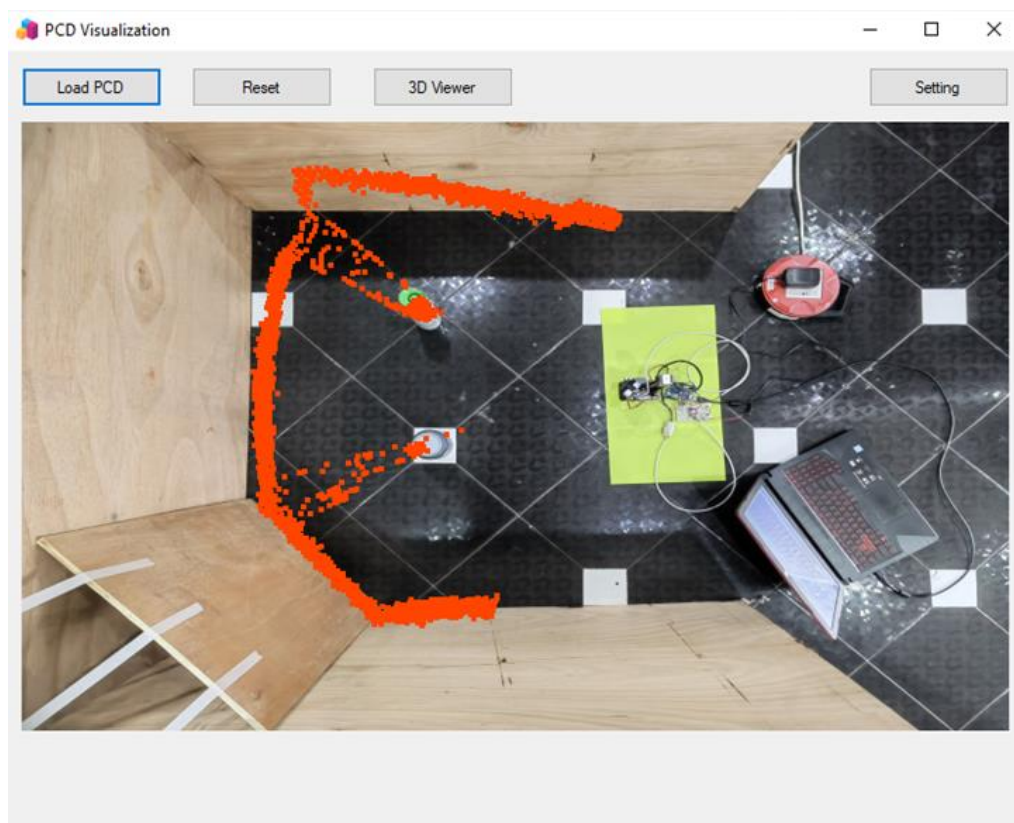


Figure 4.18: 2D viewing of point cloud overlay on image

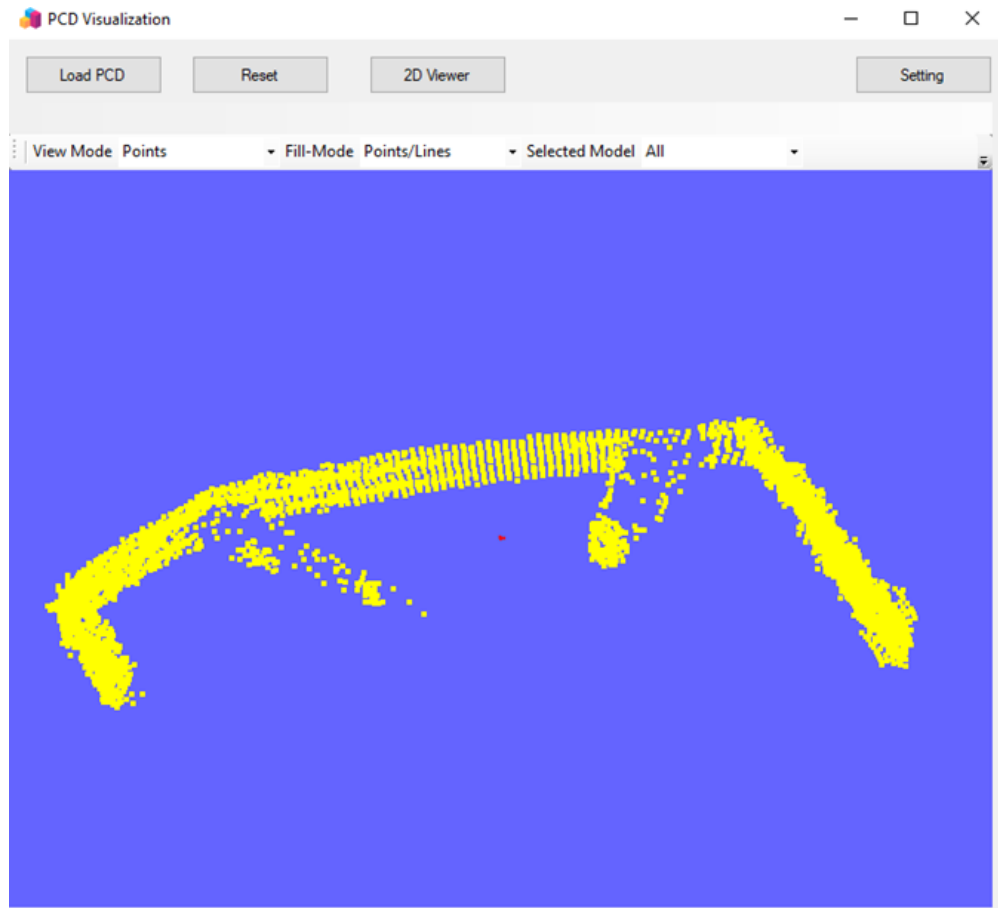


Figure 4.19: 3D viewing of point cloud

The purpose of the `LoadPointCloud()` function is to read the contents of a PCD file and generate a list of `Point3D` objects based on the data. The method initializes an empty list of points and proceeds to read the file using a `StreamReader`. The file's contents are read line by line via a while loop, and each line is split into an array of strings using the `Split` method. The delimiters are space, tab, newline, or carriage return characters. The string array is then used to extract the `x`, `y`, and `z` coordinates, which are stored in their respective variables. A new `Point3D` object is then created using these coordinate values, and it is added to the list of points. Finally, the method returns the list of points, allowing the caller to manipulate and use the point cloud data as needed. This method is a vital component of the application, as it provides a means of



importing and working with external point cloud data. Its efficient and thorough implementation is crucial to ensuring the accuracy and reliability of the program's functionality.

The `DisplayPointCloud()` function serves to generate a bitmap image and depict each point of the point cloud as a small circle on the image. The method first clears any existing points from the picture box by setting the `Image` property to null. It then creates a new `Bitmap` object with the size of the picture box. An overlay image from a file is loaded, and the position and size of the overlay image are calculated based on the picture box's dimensions. A `Graphics` object is used to draw the overlay image onto the bitmap. Next, the center point of the picture box is calculated, and each point in the point cloud is represented by a small circle drawn using a `Graphics` object. The `x` and `y` coordinates of each point are obtained from the `Point3D` object, and their values are utilized to determine the circle's position on the bitmap. Finally, the bitmap is set as the `Image` property of the picture box so that it can be displayed on the form. Additionally, the application loads an overlay image from a file and uses it as a background image for the point cloud visualization. The `DisplayPointCloud()` function is a critical aspect of the program as it allows for the point cloud to be visualized in a meaningful way. Its implementation is efficient and thorough, ensuring that the point cloud data is accurately represented on the bitmap image.

As for the 3D viewing, `OpenGL` API is being used to render the 3D point clouds. In order to utilize `OpenGL` API in this program, an open-source library is being used and it is known as `OpenTK` library (Open TK, 2021). `OpenTK`

provides OpenGL bindings and other related functionality such as window creation and input handling.

In the method named `ShowPointCloudOpenGL()`, it adds a new 3D model representing a point cloud to an existing list of models in an OpenGL control. If specified, it also removes any existing models from the control. This enables the user to display a point cloud using OpenGL graphics. The method takes two parameters: a `PointCloud` object named `myP`, which represents the point cloud to be displayed, and a boolean named `removeOthers`, which determines whether to remove any other models that are currently displayed in the OpenGL control. If `removeOthers` is true, the method first removes all models from the OpenGL control using the `RemoveAllModels` method. Then, a new `Model` object named `myModel` is created, and its `PointCloud` property is set to `myP`. The `myModel` object represents the point cloud as a 3D model. Finally, the `myModel` object is added to the `GLrender` list of the OpenGL control using the `AddModel` method. The `GLrender` list is responsible for rendering all models in the OpenGL control.

In summary, this application allows users to easily load, visualize, and manipulate point cloud data, making it a useful tool for various applications such as 3D modeling, robotics, and computer vision. The use of OpenGL and the OpenTK library adds powerful 3D visualization capabilities to the application.

## CHAPTER 5

### CONCLUSION AND RECOMMENDATION

#### 5.1 Conclusion

LiDAR, which stands for Light Detection and Ranging, is a remote sensing technology that uses laser pulses to measure distances and create precise 3D maps or models of objects, environments, or landscapes. LiDAR works by emitting rapid laser pulses and measuring the time it takes for the light to reflect off of objects and return to the sensor. This information is used to create a detailed point cloud or digital elevation model of the scanned area, which can be further processed to extract various features such as terrain elevation, vegetation density, building height, and more. LiDAR technology has numerous applications in fields such as surveying, geology, archaeology, forestry, urban planning, autonomous vehicles, and robotics.

In conclusion, the research work has successfully characterized the VCSEL laser and developed a compact LiDAR module that can perform single point distance measurement, 2D measurement, and 3D measurement with the addition of a servo motor for three-dimensional scanning. The innovative PCD visualizer enables the conversion of LiDAR data into Point Cloud Data, which can be visualized in a 3D visualizer, allowing for meaningful analysis and interpretation.

One of the main advantages of the designed compact LiDAR module is its size. The size of the VCSEL LiDAR sensor is 20mm in width, 48mm in length and 40mm in height, which its volume is only approximately 30% of the Leddar Vu8 solid-state LiDAR sensor reported in section 2.4.2 and the overall system size is on par with the solid-state LiDAR system. By focusing on reducing the size of both the laser and optical components, the created system is smaller than existing LiDAR systems on the market. This compact size allows for easy attachment to small drones or unmanned aerial vehicles (UAVs), expanding the potential applications of LiDAR technology in fields such as surveying, construction, and agriculture.

In addition, the accuracy of the VCSEL LiDAR sensor is significantly improved than the Leddar Vu8 solid-state LiDAR sensor where the VCSEL LiDAR have the accuracy of  $\pm 2\text{cm}$  and Leddar Vu8 solid-state LiDAR have an accuracy of  $\pm 5\text{cm}$ . Furthermore, the laser system has been designed to operate on low power, which reduces operation costs and makes it more environmentally friendly. This innovative approach to LiDAR technology reflects its commitment to advancing the field and addressing real-world challenges.

## 5.2 Recommendation

To improve the functionality and potential applications of the LiDAR module, it is recommended to:

1. Increase the VCSEL laser power to enable longer range sweeps to be obtained. This will expand the range of the LiDAR module and make it more versatile for a wider range of applications.
2. Implement a stepper motor to accurately obtain angle sweeps for a more precise 3D visualization. This will improve the accuracy and quality of the 3D visualization, making it more useful for various applications.
3. Implement object recognition algorithms, such as human and object detection, based on the 3D visualization including distance detection. This will enable the LiDAR module to detect and identify objects in its environment, making it more useful for safety and security applications.

By implementing these recommendations, an ultra-compact LiDAR module can be further developed that is suitable for various applications, including self-driving automotive and self-moving carts/trolleys.

## REFERENCES

Aho, A.T., Viheriälä, J., Mäkelä, J., Virtanen, H., Ranta, S., Dumitrescu, M. and Guina, M., 2017. High-power 1550 nm tapered DBR laser diodes for LIDAR applications. In: *The European Conference on Lasers and Electro-Optics*. p.CB\ 7\ 4.

ArcMap, 2023. *What is a LAS dataset?* [online] Available at: <<https://desktop.arcgis.com/en/arcmap/latest/manage-data/las-dataset/what-is-a-las-dataset-.htm>> [Accessed 15 March 2023].

Arduino, 2023. *Arduino Uno Rev3*. [online] Available at: <<https://store.arduino.cc/products/arduino-uno-rev3>> [Accessed 15 March 2023].

ASPRS, A.S. for P.& R.S., 2019. LAS Specification v. 1.4-R14.

Badamasi, Y.A., 2014. The working principle of an Arduino. In: *2014 11th international conference on electronics, computer and computation (ICECCO)*. IEEE. pp.1–4.

Bagley, H.R., Hannon, S.M., Poling, M.A. and Schnal, D.L., 1998. Air cooled flight worthy eye-safe coherent lidar transceiver. In: *17th DASC. AIAA/IEEE/SAE. Digital Avionics Systems Conference. Proceedings (Cat. No. 98CH36267)*. pp.D12--1.

Besseau, B., Pot, G., Collet, R. and Viguier, J., 2020. Influence of wood anatomy on fiber orientation measurement obtained by laser scanning on five European species. *Journal of Wood Science*, 66(1), p.74.

Booth, B. and Mitchell, A., 2001. *Getting started with ArcGIS*.

Bou Sanayeh, M., Brick, P., Schmid, W., Mayer, B., Müller, M., Reufer, M., Streubel, K., Tomm, J.W. and Bacher, G., 2007. Temperature-power dependence of catastrophic optical damage in AlGaInP laser diodes. *Applied Physics Letters*, 91(4), p.041115.

Campbell, J.R., Hlavka, D.L., Welton, E.J., Flynn, C.J., Turner, D.D., Spinhirne, J.D., Scott III, V.S. and Hwang, I.H., 2002. Full-time, eye-safe cloud and aerosol lidar observation at atmospheric radiation measurement program sites: Instruments and data processing. *Journal of Atmospheric and Oceanic Technology*, 19(4), pp.431–442.

Chickerur, S. and Joshi, K., 2015. 3D face model dataset: Automatic detection of facial expressions and emotions for educational environments. *British Journal of Educational Technology*, 46(5), pp.1028–1037.

Chung, S., Abediasl, H. and Hashemi, H., 2017. 15.4 A 1024-element scalable optical phased array in 0.18  $\mu\text{m}$  SOI CMOS. In: *2017 IEEE International Solid-State Circuits Conference (ISSCC)*. pp.262–263.

Coleman, J.J., 2012. The development of the semiconductor laser diode after the first demonstration in 1962. *Semiconductor Science and Technology*, 27(9), p.090207.

Davis, S.R., Rommel, S.D., Gann, D., Luey, B., Gamble, J.D., Ziemkiewicz, M. and Anderson, M., 2016. A lightweight, rugged, solid state laser radar system enabled by non-mechanical electro-optic beam steerers. In: *Laser Radar Technology and Applications XXI*. p.98320K.

Dethe, S.N., Shevatkar, V.S. and Bijwe, R.P., 2011. Google driverless car. *International Journal of Scientific Research in Science, Engineering and Technology*, 21(2), pp.2394–4099.

Dr. Rüdiger Paschotta, 2022. *Fiber Lasers Versus Bulk Lasers*. [online] Available at: <[https://www.rp-photonics.com/fiber\\_lasers\\_versus\\_bulk\\_lasers.html](https://www.rp-photonics.com/fiber_lasers_versus_bulk_lasers.html)> [Accessed 16 February 2023].

Feng, G., Yang, Z. and Sun, H., 2021. Highly stable erbium-doped fiber amplifier (EDFA) pumped with a constant-current-driven semiconductor laser diode (LD). In: *Twelfth International Conference on Information Optics and Photonics*. SPIE. pp.77–81.

Fersch, T., Weigel, R. and Koelpin, A., 2017. Challenges in miniaturized automotive long-range lidar system design. In: *Three-Dimensional Imaging, Visualization, and Display 2017*. p.102190T.

FindLight, 2019. *Edge Emitting vs Surface Emitting Lasers: A Comparison of Performance*. [online] Available at: <<https://www.findlight.net/blog/edge-emitting-vs-surface-emitting/>> [Accessed 14 March 2023].

Goyer, G.G. and Watson, R., 1963. The laser and its application to meteorology. *Bulletin of the American Meteorological Society*, 44(9), pp.564–570.

Hagstedt, C. and Jönsson, S., 2022. *Design and evaluation of a solid-state LiDAR system: for wireless distance measurements*.

Iga, K., 2000. Surface-emitting laser-its birth and generation of new optoelectronics field. *IEEE Journal of selected topics in Quantum Electronics*, 6(6), pp.1201–1215.

Iga, K., 2021. Semiconductor Lasers and VCSEL History. *VCSEL Industry: Communication and Sensing*, p.1.

Im, B., Baek, N. and Lee, J., 2016. An Efficient Implementation of LiDAR Data and its Geometric Representation Extraction. In: *2016 6th International Conference on IT Convergence and Security (ICITCS)*. IEEE. pp.1–4.

Isenburg, M., 2013. LASzip: lossless compression of LiDAR data. *Photogrammetric engineering and remote sensing*, 79(2), pp.209–217.

Jeong, N., Hwang, H. and Matson, E.T., 2018. Evaluation of low-cost lidar sensor for application in indoor uav navigation. In: *2018 IEEE Sensors Applications Symposium (SAS)*. pp.1–5.

Kameyama, S., Ando, T., Asaka, K., Hirano, Y. and Wadaka, S., 2007. Compact all-fiber pulsed coherent Doppler lidar system for wind sensing. *Applied optics*, 46(11), pp.1953–1962.

Kaplan, A.B., 2007. *Investigating the polarization properties of vertical-cavity surface-emitting lasers*. Citeseer.

Kim, J. and Cho, J., 2020. Exploring a multimodal mixture-of-YOLOs framework for advanced real-time object detection. *Applied Sciences*, 10(2), p.612.

Koch, S.W. and Hofmann, M.R., 2018. Semiconductor Lasers. In: B.D. Guenther and D.G. Steel, eds. *Encyclopedia of Modern Optics (Second Edition)*. [online] Oxford: Elsevier. pp.462–468. <https://doi.org/https://doi.org/10.1016/B978-0-12-803581-8.10103-1>.

Kondow, M., Kitatani, T., Nakatsuka, S., Larson, M.C., Nakahara, K., Yazawa, Y., Okai, M. and Uomi, K., 1997. GaInNAs: a novel material for long-wavelength semiconductor lasers. *IEEE Journal of selected topics in Quantum electronics*, 3(3), pp.719–730.

Koo, H., Chun, Y. and Griffith, D.A., 2018. Integrating spatial data analysis functionalities in a GIS environment: Spatial Analysis using ArcGIS Engine and R (SAAR). *Transactions in GIS*, 22(3), pp.721–736.

Koyama, F., 2006. Recent advances of VCSEL photonics. *Journal of Lightwave Technology*, 24(12), pp.4502–4513.

Larsson, A. and Gustavsson, J.S., 2013. Single-Mode VCSELs. *VCSELs: Fundamentals, Technology and Applications of Vertical-Cavity Surface-Emitting Lasers*, pp.119–144.

Lavrencik, J.J., 2020. *VCSEL-based multimode fiber optical links for high capacity interconnects*. Georgia Institute of Technology.

LeddarTech, 2023. *Leddar™ Vu8*. [online] Available at: <<https://leddarsensor.com/solutions/leddar-vu8-solid-state-lidar-sensor-module/>> [Accessed 8 August 2023].



- Lee, B., Wei, Y. and Guo, I.Y., 2017. Automatic parking of self-driving car based on lidar. *Int. Arch. Photogramm. Remote Sens. Spat. Inf. Sci.*, 42, pp.241–246.
- Levinson, J., Askeland, J., Becker, J., Dolson, J., Held, D., Kammel, S., Kolter, J.Z., Langer, D., Pink, O., Pratt, V. and others, 2011. Towards fully autonomous driving: Systems and algorithms. In: *2011 IEEE Intelligent Vehicles Symposium (IV)*. pp.163–168.
- Li, Z., Hodgson, M.E. and Li, W., 2018. A general-purpose framework for parallel processing of large-scale LiDAR data. *International Journal of Digital Earth*, 11(1), pp.26–47.
- Lidar, V., 2016. HDL-64E. *online*, [Retrieved Jul. 15, 2020]. Retrieved from Internet (10pgs).
- Lin, F.-Y. and Liu, J.-M., 2004. Chaotic lidar. *IEEE journal of selected topics in quantum electronics*, 10(5), pp.991–997.
- Liu, J., Sun, Q., Fan, Z. and Jia, Y., 2018. TOF lidar development in autonomous vehicle. In: *2018 IEEE 3rd Optoelectronics Global Conference (OGC)*. pp.185–190.
- López, J.J., Mahony, T. and Kim, S., 2020. *MIT Spinoff Building New Solid-State Lidar-on-a-Chip System*. [online] Available at: <<https://spectrum.ieee.org/kyber-photonics-solid-state-lidar-on-a-chip-system>> [Accessed 14 March 2023].
- Menzies, R.T., 1985. Coherent and incoherent lidar—an overview. In: *Tunable Solid State Lasers for Remote Sensing: Proceedings of the NASA Conference Stanford University, Stanford, USA, October 1–3, 1984*. Springer. pp.17–21.
- Mester, R., Hebel, M., Körner, E. and Rottensteiner, F., 2018. State of the art in airborne laser scanning and future trends. *ISPRS Journal of Photogrammetry and Remote Sensing*, 144, pp.166–182.
- Michalzik, R., 2013a. *VCSEL fundamentals*. Springer.
- Michalzik, R., 2013b. *VCSEL fundamentals*. Springer.
- mmolero, 2022. *awesome-point-cloud-processing*. [online] Available at: <<https://github.com/mmolero/awesome-point-cloud-processing>> [Accessed 15 March 2023].
- Moench, H., Gronenborn, S., Gu, X., Gudde, R., Herper, M., Kolb, J., Miller, M., Smeets, M. and Weigl, A., 2018. VCSELs in short-pulse operation for time-of-flight applications. In: *Vertical-Cavity Surface-Emitting Lasers XXII*. p.105520G.

Moench, H., Gronenborn, S., Gu, X., Gudde, R., Herper, M., Kolb, J., Miller, M., Smeets, M. and Weigl, A., 2019. VCSELs in short-pulse operation for time-of-flight applications. In: *Vertical-Cavity Surface-Emitting Lasers XXIII*. p.109380E.

Nelson, R., 2013. How did we get here? An early history of forestry lidar1. *Canadian Journal of Remote Sensing*, 39(sup1), pp.S6--S17.

Ng, K.L., Lim, W.X. and Teh, P.C., 2020. Implementation of 3D Mapping using A 2D LiDAR Scanner. *i-Manager's Journal on Electronics Engineering*, 10(3), p.1.

Ong, C.E., Teh, P.C., Ho, Y.K. and Chyan, L.S., 2013. Flexible optical pulse generation for laser micromachining using FPGA board with integrated high-speed DAC. *i-Manager's Journal on Digital Signal Processing*, 1(2), p.24.

Open TK, 2021. *Open TK*. [online] Available at: <<https://opentk.net/>> [Accessed 24 March 2023].

Ostermeyer, M., Kappe, P., Menzel, R. and Wulfmeyer, V., 2005. Diode-pumped Nd: YAG master oscillator power amplifier with high pulse energy, excellent beam quality, and frequency-stabilized master oscillator as a basis for a next-generation lidar system. *Applied Optics*, 44(4), pp.582–590.

Paschotta, R., 2008a. *Bandwidth*. [online] Available at: <<https://www.rp-photonics.com/bandwidth.html>> [Accessed 15 March 2023].

Paschotta, R., 2008b. *Edge-emitting Semiconductor Lasers*. [online] Available at: <[https://www.rp-photonics.com/encyclopedia\\_cite.html?article=edge-emitting%20semiconductor%20lasers](https://www.rp-photonics.com/encyclopedia_cite.html?article=edge-emitting%20semiconductor%20lasers)> [Accessed 14 March 2023].

Photonics Report, 2022. *Lidar technology: the best of remote sensing*. [online] Available at: <<https://photonicsreport.com/blog/lidar-technology-the-best-of-remote-sensing/>> [Accessed 14 March 2023].

Point Cloud Library, 2023. *The PCD (Point Cloud Data) file format*. [online] Available at: <[https://pointclouds.org/documentation/tutorials/pcd\\_file\\_format.html#pcd-file-format](https://pointclouds.org/documentation/tutorials/pcd_file_format.html#pcd-file-format)> [Accessed 15 March 2023].

Rock Academy, 2023. *Understanding LAS and LAZ File Formats*. [online] Available at: <<https://learn.rockrobotic.com/understanding-las-and-laz-file-formats>> [Accessed 15 March 2023].

Rose, K., 2018. *Materials That Absorb Infrared Rays*.

Royo, S. and Ballesta-Garcia, M., 2019. An overview of lidar imaging systems for autonomous vehicles. *Applied sciences*, 9(19), p.4093.

- rpmc, 2023. *VCSEL LASERS*. [online] Available at: <<https://www.rpmclasers.com/types/vcsels/>> [Accessed 15 March 2023].
- Rusu, R.B. and Cousins, S., 2011. 3d is here: Point cloud library (pcl). In: *2011 IEEE international conference on robotics and automation*. pp.1–4.
- Sandak, J. and Tanaka, C., 2003. Evaluation of surface smoothness by laser displacement sensor 1: Effect of wood species. *Journal of Wood Science*, 49, pp.305–311.
- Seurin, J.-F., Xu, G., Khalfin, V., Miglo, A., Wynn, J.D., Pradhan, P., Ghosh, C.L. and D’Asaro, L.A., 2009. Progress in high-power high-efficiency VCSEL arrays. In: *Vertical-Cavity Surface-Emitting Lasers XIII*. p.722903.
- Singh, H. and Bawa, S., 2016. Spatial data analysis with ArcGIS and MapReduce. In: *2016 International Conference on Computing, Communication and Automation (ICCCA)*. IEEE. pp.45–49.
- Song, J., 2014. Fabrication and Characterization of Edge-Emitting semiconductor lasers.
- Sun, W., Hu, Y., MacDonnell, D.G., Weimer, C. and Baize, R.R., 2016. Technique to separate lidar signal and sunlight. *Optics express*, 24(12), pp.12949–12954.
- Szewrański, S., Kazak, J., Sylla, M. and Świąder, M., 2017. Spatial data analysis with the use of ArcGIS and Tableau systems. In: *The Rise of big spatial data*. Springer. pp.337–349.
- Takeuchi, N., Baba, H., Sakurai, K. and Ueno, T., 1986. Diode-laser random-modulation cw lidar. *Applied optics*, 25(1), pp.63–67.
- Tommy Mi, 2022. *Innovations of Autonomous Vehicles: Solid-State LiDAR Sensors*. [online] Available at: <<https://www.equalocean.com/analysis/2022031917148>> [Accessed 16 February 2023].
- Trumpf, 2021. *VCSEL solutions for 3D sensing applications*.
- Wandinger, U., 2005. Introduction to lidar. In: *Lidar*. Springer. pp.1–18.
- Weigl, B., Grabherr, M., Jung, C., Jager, R., Reiner, G., Michalzik, R., Sowada, D. and Ebeling, K.J., 1997. High-performance oxide-confined GaAs VCSELs. *IEEE Journal of Selected Topics in Quantum Electronics*, 3(2), pp.409–415.
- Winiwarter, L., Pena, A.M.E., Weiser, H., Anders, K., Sánchez, J.M., Searle, M. and Höfle, B., 2022. Virtual laser scanning with HELIOS++: A novel take on ray tracing-based simulation of topographic full-waveform 3D laser scanning. *Remote Sensing of Environment*, 269, p.112772.

Wu, Z., Zeng, Y., Li, D., Liu, J. and Feng, L., 2021. High-volume point cloud data simplification based on decomposed graph filtering. *Automation in Construction*, 129, p.103815.

Yablonovitch, E. and Kane, E.O., 1988. Band structure engineering of semiconductor lasers for optical communications. *Journal of lightwave technology*, 6(8), pp.1292–1299.

Yamada, M., 1983. Transverse and longitudinal mode control in semiconductor injection lasers. *IEEE Journal of Quantum Electronics*, 19(9), pp.1365–1380.

Zeng, Z., Sun, K., Wang, G., Zhang, T., Kulis, S., Gui, P. and Moreira, P., 2017. A compact low-power driver array for VCSELs in 65-nm CMOS technology. *IEEE Transactions on Nuclear Science*, 64(6), pp.1599–1604.

Zhang, J., Ning, Y., Zhang, X., Hofmann, W., Liu, K., Zhang, J., Qiu, J., Zeng, Y., Fu, X., Huang, Y. and others, 2018. 910 nm vertical-cavity surface-emitting laser arrays with 100 W output power level and low driving current. *Japanese Journal of Applied Physics*, 57(10), p.100302.

Zhou, D., Seurin, J.-F., Xu, G., Van Leeuwen, R., Miglo, A., Wang, Q., Kovsh, A. and Ghosh, C., 2017. Progress on high-power 808nm VCSELs and applications. In: *Vertical-Cavity Surface-Emitting Lasers XXI*. SPIE. pp.33–41.

## APPENDICES

### Appendix A: Coding for Arduino Microcontroller

```
#include <Servo.h>

Servo myservo; // create servo object to control a servo

//Define variables
int pos = 0;
int i = 0;
int m = 0;
int avgPoint = 1;
unsigned long pulseWidth;
unsigned long totDistance = 0;
unsigned long avgDistance = 0;
float xPos;
float yPos;
float zPos = 0;
float Pi = 3.1416;

// Define pin connections
const int triggerPin = 2; // Set pin 2 as Lidar lite trigger pin
const int monitorPin = 3; // Set pin 3 as Lidar lite monitor pin
const int servoPin = 10; // Set pin 10 as servo motor pwm pin
const int dirPin = 8; // Set pin 8 as stepper motor direction pin
const int stepPin = 9; // Set pin 9 as stepper motor pulse pin

void setup()
{
  Serial.begin(115200); // Start serial communications

  myservo.attach(servoPin); // attaches the servo on pin 6 to the servo object

  // Declare pins as Inputs & Outputs
  pinMode(triggerPin, OUTPUT); // Set pin 2 (trigger pin) as output
  digitalWrite(triggerPin, LOW); // Set trigger LOW for continuous read
  pinMode(monitorPin, INPUT); // Set pin 3 (monitor pin) as input
  pinMode(dirPin, OUTPUT); // Set pin 8 (stepper direction) as output
  pinMode(stepPin, OUTPUT); // Set pin 9 (stepper pulse) as output
}

void loop()
{
  if (pos == 0)
  {
    myservo.write(pos); // tell servo to go to position in variable 'pos'
    delay(500);
  }

  // Reset the servo and move up
```

```

if (pos == 181)
{
  pos = 0; // Reset pos
  myservo.write(pos); // tell servo to go to position in variable 'pos'
  delay(500);
  m++; // m increment
  MoveUp0; // Move up by 5mm

  // Reset z position
  if (m == 25)
  {
    m = 0; // Reset m
    MoveDown0; // Move down to starting position
  }
}

myservo.write(pos); // tell servo to go to position in variable 'pos'
delay(15);

pulseWidth = pulseIn(monitorPin, HIGH); // Count how long the pulse is
high in microseconds

// If reading not zero, calculate distance
if(pulseWidth != 0)
{
  pulseWidth = pulseWidth / 10; // 10usec = 1 cm of distance
}

i++; // i increment
totDistance = totDistance + pulseWidth; // Continue adding the readings

// Calculate the average reading
if (i == avgPoint)
{
  avgDistance = totDistance / avgPoint; // Divide the total distance by the
number of points

  xPos = avgDistance * cos(pos*(Pi/180)); // Convert and get the x-coordinate
  Serial.print(xPos); // Print the x-coordinate
  Serial.print(" ");

  yPos = avgDistance * sin(pos*(Pi/180)); // Convert and get the y-coordinate
  Serial.print(yPos); // Print the y-coordinate
  Serial.print(" ");

  zPos = m * 0.5; // 5mm for every moving, z-coordinate
  Serial.println(zPos); // Print the z-coordinate

  i = 0; // Reset i
  totDistance = 0; // Reset average distance
  pos++; // pos increment
}
}

void MoveUp0

```

```

{
// Set motor direction
digitalWrite(dirPin, LOW);

// Start motor
for(int d = 0; d < 79; d++)
{
digitalWrite(stepPin, HIGH);
delayMicroseconds(4000);
digitalWrite(stepPin, LOW);
delayMicroseconds(4000);
}
delay(1000); // Wait 1 second
}

void MoveDown()
{
// Set motor direction
digitalWrite(dirPin, HIGH);

// Start motor
for(int d = 0; d < 1975; d++)
{
digitalWrite(stepPin, HIGH);
delayMicroseconds(4000);
digitalWrite(stepPin, LOW);
delayMicroseconds(4000);
}
delay(1000); // Wait 1 second
}

```